Europium Oxybromide Catalysts for Efficient Bromine Looping in Natural Gas Valorization

Author(s):
Paunović, Vladimir; Lin, Ronghe; Scharfe, Matthias; Amrute, Amol P.; Mitchell, Sharon; Hauert, Roland; Pérez-Ramírez, Javier

Publication date:
2017-08

Permanent link:
https://doi.org/10.3929/ethz-b-000190524

Originally published in:
Angewandte Chemie. International Edition 56(33), https://doi.org/10.1002/anie.201704406

Funding acknowledgement:
156107 - Design of oxyhalogenation catalysts for hydrocarbon functionalization (SNF)

Europium Oxybromide Catalysts for Efficient Bromine Looping in Natural Gas Valorization

Vladimir Paunović[+], Ronghe Lin[+], Matthias Scharfe, Amol P. Amrute, Sharon Mitchell, Roland Hauert, and Javier Pérez-Ramírez*

Abstract: The industrialization of bromine-mediated natural gas upgrading is contingent on the ability to fully recycle hydrogen bromide (HBr), which is the end form of the halogen after the activation and coupling of the alkanes. Europium oxybromide (EuOBr) is introduced as a unique catalytic material to close the bromine loop via HBr oxidation, permitting low-temperature operation and long lifetimes with a stoichiometric feed (O_2:HBr = 0.25), conditions at which any catalyst reported to date severely deactivates due to excessive bromination. Besides, EuOBr exhibits unparalleled selectivity to methyl bromide in methane oxybromination, an alternative route for bromine looping. This novel active phase is finely dispersed on appropriate carriers and scaled up to technical extrudates, enhancing the utilization of europium by over an order of magnitude while preserving the performance. This catalytic system paves the way for the sustainable valorization of stranded natural gas via bromine chemistry.

More than 30% of the known world's natural gas reserves are located in remote and scattered wells.[1] This fact precludes their use as a long-lasting feedstock for the manufacture of chemicals and fuels due to the prohibitive shipping expenses to centralized megaplants.[2] Consequently, natural gas emitted from these wells is nowadays flared or vented, wasting ca. 3.5% of its global production, which is a fraction worth 13 billion USD.[3] Among the various routes proposed to overcome the capital intensity of conventional syngas-based processes,[4] the bromine-mediated functionalization of methane into methyl bromide (CH_3Br), a versatile C1 platform molecule with similar upgrading paths to methanol, emerged as an economically attractive technology for the decentralized manufacture of readily transportable value-added chemicals and fuels in compact plants amenable to decentralization.[2,5-10] Key steps of the process (**Figure 1**, **Figure S1**),[2,6-9] which could also be applied to ethane and propane,[2] comprise (1) methane bromination, which provides up to 95% selectivity to CH_3Br, (2) reproportionation of the polybrominated byproducts into monobrominated alkanes and olefins by reaction with C1-C5 alkanes, (3) coupling of CH_3Br and reproportionation products into valuable hydrocarbons such as gasolines, olefins, and aromatics, and (4) recycling of hydrogen bromide (HBr), which is generated in stoichiometric amounts in the bromination and coupling steps. The latter step closes the bromine loop and is vital to the feasibility of the entire technology, since the high price and low availability of this halogen necessitate its full recovery. The highly efficient carbon atom utilization enabled by developments in the bromination, reproportionation, and coupling reactions, as well as advances in corrosion resistant construction materials led to a large-scale demonstration of the bromine-based process for the production of petrochemical-grade aromatics from methane, which is nowadays offered for licensing.[2,10] Nevertheless, little progress has been made towards sustainable bromine looping, which is commonly accomplished via cataloreactant processes or the catalytic HBr oxidation.[2,8,11] The former approach relies on the absorption of HBr by an oxide or hydroxide, followed by its re-oxidation in a second step to evolve bromine. However, such a cyclic operation necessitates large reactors and is difficult to control due to the limited lifetime of the cataloreactants. Hence, it is highly desirable to develop a catalytic system for the continuous oxidation of HBr into molecular bromine at relatively low temperatures ($T \leq 573$ K) and stoichiometric feed (O_2:HBr = 0.25). In addition to enhancing the overall space-time and energy efficiency of the process, this would enable the use of air as an oxygen source, thereby substantially reducing production costs. Nevertheless, such an operating window remains highly challenging due to the extensive bromination of active catalysts like RuO_2 and CeO_2 even under significant oxygen excess, leading to severe deactivation.[11c,d]

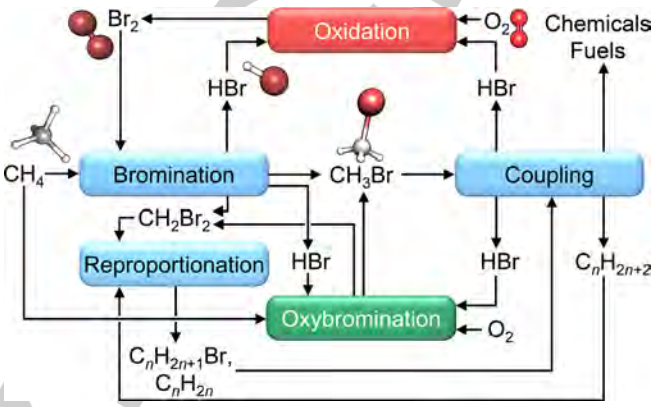

Figure 1. Process flow diagram of bromine-mediated natural gas upgrading.

In our quest for a novel catalytically active phase enabling efficient bromine looping, we have investigated the performance of various rare-earth oxides comprising La_2O_3, Sm_2O_3, Eu_2O_3, Gd_2O_3, Tb_2O_3, and Dy_2O_3 in HBr oxidation. Catalysts based on

[*] V. Paunović[+], Dr. R. Lin[+], M. Scharfe, Dr. A. P. Amrute, Dr. S. Mitchell, Prof. J. Pérez-Ramírez
Institute for Chemical and Bioengineering
Department of Chemistry and Applied Biosciences, ETH Zurich
Vladimir-Prelog-Weg 1, 8093 Zurich, Switzerland
E-mail: jpr@chem.ethz.ch

Dr. R. Hauert
Empa, Swiss Federal Laboratories for Materials Science and Technology
Überlandstrasse 129, 8600 Dübendorf, Switzerland

[+] Equal contribution

Supporting information for this article is given via a link at the end of the document.

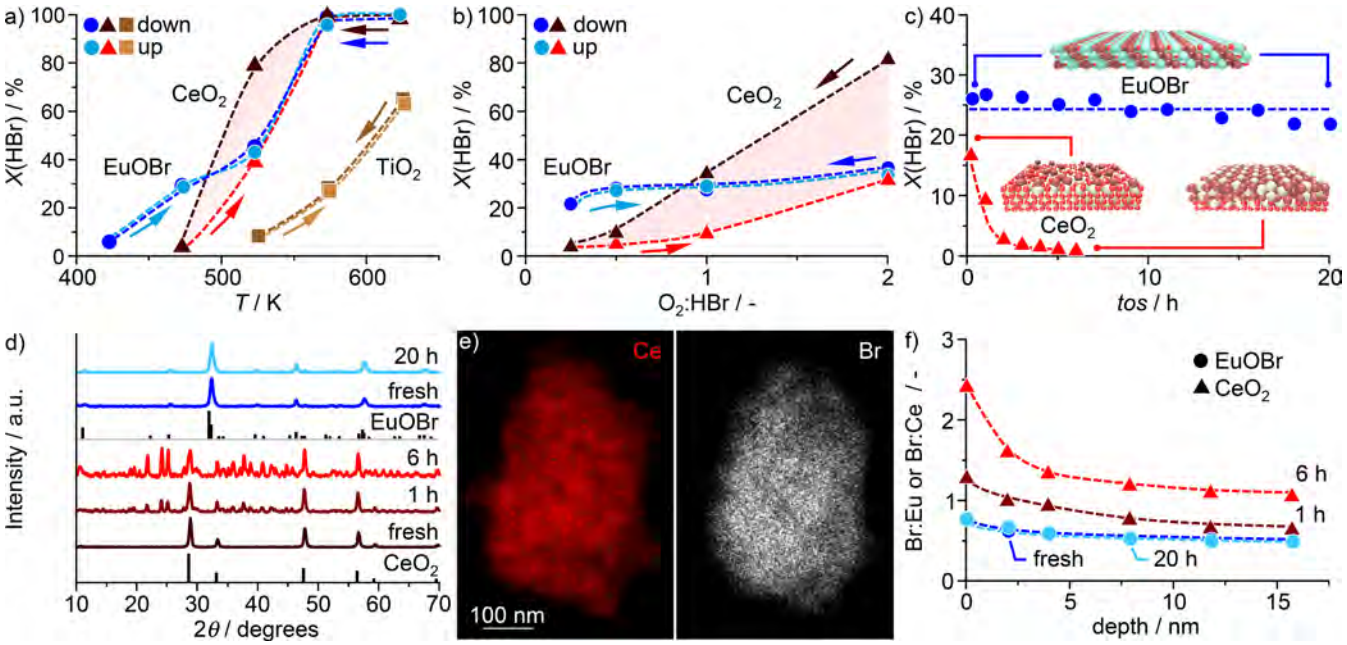

Figure 2. HBr conversion, *X*(HBr), over different catalysts *versus*: a) temperature, *T*, at a molar O_2:HBr ratio of 2, b) molar O_2:HBr ratio at *T* = 523 K, and c) time-on-stream, *tos*, at *T* = 523 K and a stoichiometric O_2:HBr ratio of 0.25 (O_2:HBr = 0.25). Temperature and O_2:HBr ratio were decreased from the highest to the lowest value (down), and then increased back to the starting point (up). The colored areas in a) and b) indicate the pronounced deactivation hysteresis of CeO_2. d) X-ray diffractograms of EuOBr (top) and CeO_2 (bottom) samples recovered after various time-on-stream (O_2:HBr = 0.25, *T* = 523 K). Patterns of the reference EuOBr (ICDD-PDF 85-0844) and CeO_2 (ICDD-PDF 81-0792) phases are presented with vertical lines. e) Energy dispersive X-ray spectroscopy elemental maps of CeO_2 catalyst recovered after 1 h of operation (O_2:HBr = 0.25, *T* = 523 K) testify its excessive bromination. f) X-ray photoelectron spectroscopy depth profiles of EuOBr and CeO_2 samples recovered after various time-on-stream (O_2:HBr = 0.25, *T* = 523 K) demonstrate a constant atomic Br:Eu ratio and a progressive increase in Br:Ce ratio in the surface region of the respective catalysts, as illustrated in c). Conditions: HBr:O_2:He = 4.5:1.13-9:94.37-86.5, space velocity, F_T/W_{cat} = 200 $cm^3\ min^{-1}\ g_{cat}^{-1}$, *P* = 1 bar.

lanthanide metals have been widely applied in numerous reactions,[13] but apart from CeO_2, no member of this catalyst family has been investigated in HBr oxidation. Initial catalytic tests were conducted using an oxygen-rich feed (O_2:HBr = 2), which favors the re-oxidation of the catalyst (see the Supporting Information, **Figure S4**).[11c,d] All of the catalysts were found to transform to the oxybromide phase under these conditions (**Figure S3**). Consequently, the performance of the lanthanide oxybromide phases was considered henceforth. Comparatively, the highest rates of HBr oxidation in the low-temperature window (423-473 K) were observed over EuOBr, substantially exceeding those of the benchmark CeO_2 and TiO_2 catalysts (**Figure 2a**, **Figure S4**). To the best of our knowledge, this is the first report on the application of EuOBr in catalysis. The light-off curve of LaOBr was shifted to ca. 150 K higher temperature compared to EuOBr. Besides, it suffered deactivation (**Figure S4**). Other lanthanide oxybromides were all active at temperatures (*T* > 623 K), exceeding the preferred operating window.

The performance of EuOBr remained unaltered upon temperature cycling (**Figure 2a**), which simulates the likely spatial and temporal fluctuations in a reactor. In contrast, during the temperature-increasing part of cycle CeO_2 displayed a lower HBr conversion than during the temperature-decreasing part, indicating deactivation caused by a bromine uptake at low temperatures.[11c,d] On the other hand, TiO_2, which is the benchmark of the bromination-resistant catalysts,[11b,d] was much less active compared to EuOBr. The stability of the latter material was also evidenced on cycling the feed concentration of oxygen (**Figure 2b**). Notably, the performance of EuOBr was only slightly affected by the oxygen concentration, showing no deactivation. Contrarily, the conversion of HBr over CeO_2 drops to almost zero under the preferred stoichiometric feed (O_2:HBr = 0.25), and is only partially recovered upon returning to higher oxygen concentrations. The outstanding robustness of EuOBr was further demonstrated by its stable activity in a time-on-stream test under stoichiometric feed at 523 K (**Figure 2c**). Under the same conditions, the bromine production over CeO_2 almost completely ceased just after 6 h. The deactivation profiles of this material observed upon temperature and oxygen cycling, as well as with time-on-stream coincide with the behavior of other highly active catalysts in this reaction such as RuO_2.[11c,d]

The contrasting performance of EuOBr and CeO_2 was rationalized by in-depth characterization of the catalysts recovered after different time-on-stream in HBr oxidation. The appearance of new reflections in the X-ray diffraction patterns of the used samples evidenced the chemical transformation of CeO_2 (**Figure 2d**), which based on the increasing degree of bromination (vide infra) was tentatively ascribed to the formation of (oxy)bromide phases (**Figure S6**). Besides, pronounced particle sintering was evidenced from a drop in surface area of the catalyst recovered after 6 h of reaction (13 $m^2\ g^{-1}$) with respect to the fresh material (27 $m^2\ g^{-1}$) which was also supported by electron microscopy examination (**Figure S7**). Remarkably, the bulk structure of EuOBr showed no significant change after 20 h of use (**Figure 2d, Figure S7**), whereby its surface area (19 $m^2\ g^{-1}$) was slightly lower compared to the fresh catalyst (22 $m^2\ g^{-1}$). The profound resistance of EuOBr to further bromination and the progressive uptake of bromine by CeO_2 are evidenced by the elemental maps obtained using energy

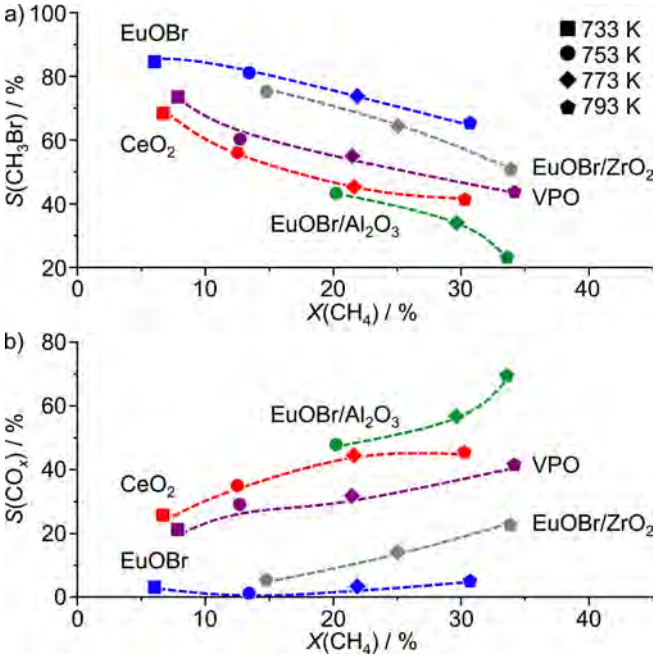

Figure 3. Selectivity to a) CH_3Br, $S(CH_3Br)$, and b) carbon oxides, $S(CO_x)$, *versus* CH_4 conversion, $X(CH_4)$, in MOB over bulk EuOBr, CeO_2, and VPO, and supported $EuOBr/ZrO_2$ and $EuOBr/Al_2O_3$ catalysts at various temperatures. Conditions: CH_4:HBr:O_2:Ar:He = 6:6:3:4.5:80.5, F_T/W_{cat} = 100 cm^3 min^{-1} g_{cat}^{-1}, P = 1 bar. The legend in a) also applies in b).

dispersive X-ray spectroscopy (**Figure 2e**, **Figure S7**), and thermogravimetric analysis (**Figure S8**). Inspection of the fresh and used CeO_2 by X-ray photoelectron spectroscopy further demonstrated the increase of bromine content in the surface region of this catalyst upon use (**Figure 2f**), leading to its reduction (**Figure S9**), ultimately resulting in its deactivation (**Figure 2c**). On the other hand, EuOBr displayed a constant Br:Eu ratio of ca. 0.7 in the surface region (**Figure 2f**), confirming the ability of EuOBr to preserve an excess of oxygen under stoichiometric feed. Europium was found to predominantly exist as Eu^{3+} with a minor contribution of Eu^{2+} (**Figure S10**), suggesting the Eu^{3+}/Eu^{2+} redox couple to be responsible for the catalyst activity. Based on these results, the exceptional stability of EuOBr can be ascribed to the structural integrity of this phase, which is preserved in oxygen-rich and HBr-rich feed mixture.

Given the outstanding performance in HBr oxidation, EuOBr was further evaluated in methane oxybromination (MOB), which is an alternative option to accomplish a continuous bromine looping by integrating HBr oxidation and methane functionalization in a single step (**Figure 1**, **Figure S1**).[12] Besides stability and activity constraints, another challenging aspect in the design of a MOB catalyst is to attain a high selectivity to CH_3Br by suppressing the side combustion reactions.[12] The latter are avoided if methane bromination and HBr oxidation are executed separately, which favors the two-step route over MOB. Notably, the selectivity to CH_3Br over EuOBr (85-65% at 6-33% single-pass methane conversion) substantially exceeded that of the benchmark $(VO)_2P_2O_7$ (VPO) and CeO_2 catalysts at comparable reaction rates in the broad range of conditions applied (**Figure 3**, **Figure S11**).[12]. EuOBr also provided the highest selectivity to CH_3Br (7-56%) and CH_2Br_2 (2-30%) on the basis of HBr (51-95% single-pass conversion), although the selectivity to bromine (17-90%) was significant (17-90%) (**Figure S12**). Moreover, it exhibited a low formation of carbon oxides (CO_x), yielding bromine and dibromomethane (CH_2Br_2) as the dominant byproducts, which can be further upgraded via bromination and reproportionation, respectively (**Figure 1**, **Figure S1**).[2,9]

To rationalize the activity of EuOBr in MOB, the catalyst was evaluated in methane combustion and methane bromination (**Figure S13**), which were chosen as the test reactions to probe the catalyst ability to dissociate C-H and form C-Br bonds, respectively. The low activity of EuOBr in methane combustion and absence of its catalytic effect in methane bromination, suggest a low propensity of this material to activate this alkane. Besides, MOB over EuOBr proceeds in the same temperature window (T > 733 K) as the non-catalytic gas-phase bromination of methane, whereby the two reactions exhibit almost identical apparent activation energy (**Figure S13**). It is thus proposed that MOB proceeds by the gas-phase reaction of methane with molecular bromine that is (re)generated by the HBr oxidation on EuOBr.[12b,c] The highly suppressed CO_x formation over this catalyst also agrees with its low propensity to combust methane.

Having identified the outstanding properties of EuOBr in HBr oxidation and MOB, the next step was to develop a ready-to-use technical catalyst based on this material. Besides reducing the price of a catalyst, the dispersion of an active phase over a suitable carrier can improve the intrinsic activity by ensuring both a high surface area and favorable electronic interaction. To study the potential impact of active phase dispersion, EuOBr was supported on three carriers: Al_2O_3, ZrO_2, and SiO_2 (9 wt.% europium loading) yielding catalysts denoted as $EuOBr/Al_2O_3$, $EuOBr/ZrO_2$, and $EuOBr/SiO_2$, respectively. These were evaluated in HBr oxidation revealing the following activity trend: $EuOBr/Al_2O_3$ > $EuOBr/ZrO_2$ > $EuOBr/SiO_2$ (**Figure 4a**), Notably, the conversion of HBr over $EuOBr/Al_2O_3$ substantially exceeded that of the bulk system in the low-temperature region, *i.e.* enabling over one order of magnitude higher rate of HBr oxidation per content of europium, while preserving its resistance against bromination (**Figure S13**). Characterization of

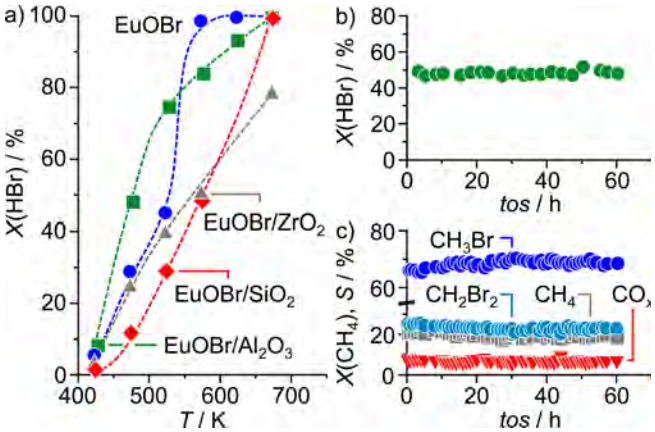

Figure 4. a) HBr conversion *versus* temperature in HBr oxidation over bulk EuOBr and supported $EuOBr/Al_2O_3$, $EuOBr/ZrO_2$, and $EuOBr/SiO_2$ catalysts (HBr:O_2:He = 4.5:9:86.5, F_T/W_{cat} = 200 cm^3 min^{-1} g_{cat}^{-1}). b) HBr conversion *versus* time-on-stream in HBr oxidation over $EuOBr/Al_2O_3$-t catalyst (HBr:O_2:He = 10:2.5:87.5, F_T/W_{cat} = 50 cm^3 min^{-1} g_{cat}^{-1}, T = 523 K). c) CH_4 conversion and product selectivity *versus* time-on-stream in MOB over $EuOBr/ZrO_2$-t catalyst (CH_4:HBr:O_2:Ar:He = 6:6:2:4.5:81.5, F_T/W_{cat} = 200 cm^3 min^{-1} g_{cat}^{-1}, T = 773 K).

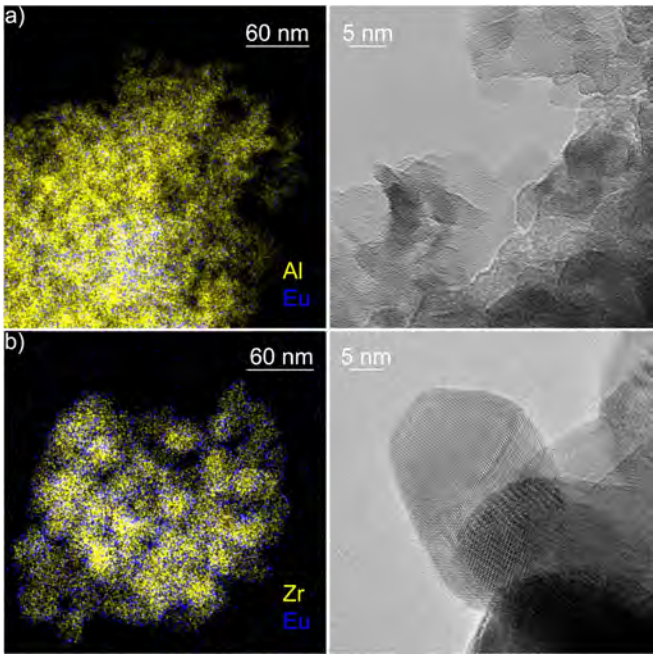

Figure 5. Energy dispersive X-ray spectroscopy elemental maps (left) and high-resolution transmission electron micrographs (right) of the a) $EuOBr/Al_2O_3$ and b) $EuOBr/ZrO_2$ catalysts used in the HBr oxidation tests indicate the high and uniform dispersion of the active phase.

the fresh and used samples revealed an atomic level dispersion of europium over all supported catalysts (**Figure 5**, **Figures S15**,**S16**). The specific surface area of the best performing $EuOBr/Al_2O_3$ was intermediate between that of $EuOBr/ZrO_2$ and $EuOBr/SiO_2$ (**Table S3**), suggesting that the observed activity trend is also affected by the specific interaction with the support. On the other hand, the degree of bromination, ability to evolve bromine, and reducibility of the supported catalysts, which all decrease in the order: $EuOBr/Al_2O_3 > EuOBr/ZrO_2 >> EuOBr/SiO_2$ (**Figures S16**,**S17**, **S18**), strongly correlate with the activity in HBr oxidation. This confirms the impact of the carrier identity on the susceptibility to bromination, whereby the supported systems with a bromine content close to that of the oxybromide display a higher activity in HBr oxidation. The outstanding performance of $EuOBr/Al_2O_3$ was thus rationalized by the ability of Al_2O_3 to stabilize the brominated form the catalyst and to promote the bromine evolution with respect to the bulk system.

In the case of MOB, the supported systems led to an increased production of CO_x with respect to bulk EuOBr (**Figure 3**, **Figure S19**). This was particularly pronounced over $EuOBr/Al_2O_3$, which could be attributed to its high oxidizing potential (**Figure S18**) as well as the propensity of Al_2O_3 to combust halocarbons.[14] On the other hand, an enhanced CO_x formation over $EuOBr/SiO_2$ is consistent with the low degree of the catalyst bromination, which promotes combustion.[12c] $EuOBr/ZrO_2$ shows balanced redox properties and a relatively high degree of bromination, providing the highest selectivity to CH_3Br among the supported systems, which is close to that of the bulk EuOBr and is also preserved at lower Eu loading (**Figure S20**).

Based on the relative performance of the supported systems, Al_2O_3 and ZrO_2 extrudates were chosen to prepare technical catalysts (*i.e.* $EuOBr/Al_2O_3$-t and $EuOBr/ZrO_2$-t), which were tested in the low-temperature HBr oxidation and MOB under stoichiometric, and substoichiometric feeds, respectively. Their activity matched that of the supported systems in powder form and was stable for over 60 h of operation under these harsh conditions (**Figure 4b,c**), with no detectable loss of europium.

In conclusion, EuOBr was found to be an exceptional catalyst for HBr oxidation, enabling low-temperature operation under a stoichiometric feed, conditions inaccessible to existing systems. This was ascribed to the marked bromine evolution activity and inherent resistance to further bromination of the oxybromide phase. Moreover, this material provided a high selectivity to CH_3Br in MOB, outperforming all previously reported catalysts. The substantially suppressed CO_x production over EuOBr opens the door for the development of catalytic systems that do not produce these side products. Thereby, the conversion of CH_2Br_2 via reproportionation could further enhance the overall selectivity to CH_3Br. To bridge the gap between the activity of EuOBr in bromine recovery processes and its high price, the impact of different carriers on its performance was investigated. Al_2O_3 and ZrO_2 were identified as the best supports for HBr oxidation and MOB, respectively, enabling an order of magnitude improved utilization of europium compared to the bulk catalyst. Technical catalysts prepared using the latter supports displayed robust performance demonstrating their realistic potential for application in bromine-based processes that can enable the decentralized valorization of stranded natural gas.

Experimental Section

Details of the catalyst preparation, characterization, and evaluation are provided as Supporting Information.

Acknowledgements

The Swiss National Science Foundation (project no. 200021-156107) for funding and ScopeM at ETH Zurich for access to their facilities.

Keywords: bromine looping • C1 chemistry • europium oxybromide • heterogeneous catalysis • natural gas upgrading

[1] a) J. A. Labinger, J. E. Bercaw, *Nature* **2002**, *417*, 507-514; b) R. Khalilpour, I. A. Karimi, *Energy* **2012**, *40*, 317-328.

[2] a) E. McFarland, *Science* **2012**, *338*, 340-342; b) R. Lin, A. P. Amrute, J. Pérez-Ramírez, *Chem. Rev.* **2017**, *117*, 4182-4247.

[3] a) J. Tollefson, *Nature* **2016**, DOI:10.1038/nature.2016.19141; b) U.S. Energy Information Administration, *Monthly Energy Review, June 2016*, U.S. Department of Energy, Washington, U.S., **2016**.

[4] a) T. Ito, J. H. Lunsford, *Nature* **1985**, *314*, 721-722; b) R. A. Periana, D. J. Taube, S. Gamble, H. Taube, T. Satoh, H. Fujii, *Science* **1998**, *280*, 560-564; c) X. G. Guo, G. Z. Fang, G. Li, H. Ma, H. J. Fan, L. Yu, C. Ma, X. Wu, D. H. Deng, M. M. Wei, D. L. Tan, R. Si, S. Zhang, J. Q. Li, L. T. Sun, Z. C. Tang, X. L. Pan, X. H. Bao, *Science* **2014**, *344*, 616-619; d) S. Grundner, M. A. C. Markovits, G. Li, M. Tromp, E. A. Pidko, E. J. M. Hensen, A. Jentys, M. Sanchez-Sanchez, J. A. Lercher, *Nat. Commun.* **2015**, *6*, 7546; e) R. Horn, R. Schlögl, *Catal. Lett.* **2015**, *145*,

23-39; f) S. H. Morejudo, R. Zanon, S. Escolastico, I. Yuste-Tirados, H. Malerod-Fjeld, P. K. Vestre, W. G. Coors, A. Martinez, T. Norby, J. M. Serra, C. Kjolseth, *Science* **2016**, *353*, 563-566; g) P. Tomkins, A. Mansouri, S. E. Bozbag, F. Krumeich, M. B. Park, E. M. C. Alayon, M. Ranocchiari, J. A. van Bokhoven, *Angew. Chem. Int. Ed.* **2016**, *55*, 5467-5471; *Angew. Chem.* **2016**, *128*, 5557-5561; h) W. Taifan, J. Baltrusaitis, *Appl. Catal. B Environ.* **2016**, *198*, 525–547; i) E. V. Kondratenko, T. Peppel, D. Seeburg, V. A. Kondratenko, N. Kalevaru, A. Martin, S. Wohlrab, *Catal. Sci. Technol.* **2017**, *7*, 366-381.

[5] a) G. A. Olah, B. Gupta, M. Farina, J. F. Felberg, W. M. Ip, A. Husain, R. Karpeles, K. Lammertsma, A. K. Melhotra, N. J. Trivedi, *J. Am. Chem. Soc*. **1985**, *107*, 7097-7105; b) V. Degirmenci, A. Yilmaz, D. Uner, *Catal. Today* **2009**, *142*, 30–33.

[6] a) I. Lorkovic, M. Noy, M. Weiss, J. Sherman, E. McFarland, G. D. Stucky, P. C. Ford, *Chem. Commun.* **2004**, 566-567; b) I. M. Lorkovic, S. L. Sun, S. Gadewar, A. Breed, G. S. Macala, A. Sardar, S. E. Cross, J. H. Sherman, G. D. Stucky, P. C. Ford, *J. Phys. Chem. A* **2006**, *110*, 8695-8700; c) K. L. Ding, H. Metiu, G. D. Stucky, *ACS Catal.* **2013**, *3*, 474-477.

[7] a) S. Svelle, S. Aravinthan, M. Bjorgen, K. P. Lillerud, S. Kolboe, I. M. Dahl, U. Olsbye, *J. Catal.* **2006**, *241*, 243-254; b) A. Zhang, S. Sun, Z. J. Komon, N. Osterwalder, S. Gadewar, P. Stoimenov, D. J. Auerbach, G. D. Stucky, E. W. McFarland, *Phys. Chem. Chem. Phys.* **2011**, *13*, 2550-2555.

[8] a) X. P. Zhou, I. M. Lorkovic, G. D. Stucky, P. C. Ford, J. H. Sherman, P. Grosso (GTR, Inc., The Regents of the University of California), US-B1 6472572, **2002**; b) J. J. Waycuilis (Marathon Oil Company), US-B2 7244867, **2007**; c) S. Gadewar, S. A. Sardar, P. Grosso, A. Zhang, V. Julka, P. Stolmanov (Baker Botts L.L.P), US-A1 2010/0096588, **2010**.

[9] a) I. M. Lorkovic, S. Sun, S. Gadewar, A. Breed, G. S. Macala, A. Sardar, S. E. Cross, J. H. Sherman, G. D. Stucky, P. C. Ford, *J. Phys. Chem. A* **2006**, *110*, 8695–8700; b) H. L. H. Fong, R. D. Swain (Shell Oil Company), US-A1 2010/0234637, **2010**.

[10] GTC Technology, 2017. Gas to Aromatics - GT-G2A, www.gtctech.com, accessed April 12th, **2017**,10:00 GMT.

[11] a) M. Moser, L. Rodríguez-García, A. P. Amrute, J. Pérez-Ramírez, *ChemCatChem* **2013**, *5*, 3520-3523; b) M. Moser, I. Czekaj, N. López, J. Pérez-Ramírez, *Angew. Chem. Int. Ed*. **2014**, *53*, 8628-8633; *Angew. Chem.* **2014**, *126*, 8772-8777; c) M. Moser, G. Vilé, S. Colussi, F. Krumeich, D. Teschner, L. Szentmiklósi, A. Trovarelli, J. Pérez-Ramírez, *J. Catal.* **2015**, *331*, 128-137; d) M. Moser, V. Paunović, Z. Guo, L. Szentmiklósi, M. G. Hevia, M. Higham, N. López, D. Teschner, J. Pérez-Ramírez, *Chem. Sci*. **2016**, *7*, 2996-3005.

[12] a) J. He, T. Xu, Z. Wang, Q. Zhang, W. Deng, Y. Wang, *Angew. Chem. Int. Ed.* **2012**, *51*, 2438-2442; *Angew. Chem.* **2012**, *124*, 2488-2492; b) V. Paunović, G. Zichittella, M. Moser, A. P. Amrute, J. Pérez-Ramírez, *Nat. Chem*. **2016**, *8*, 803-809; c) G. Zichittella, V. Paunović, A. P. Amrute, J. Pérez-Ramírez, *ACS Catal.* **2017**, *7*, 1805-1817.

[13] a) S. Park, J. M. Vohs, R. J. Gorte, *Nature* **2000**, *404*, 265-267; b) R. J. Gorte, *AIChE J.* **2010**, *56*, 1126-1135; c) C. A. Gartner, A. C. van Veen, J. A. Lercher, *ChemCatChem* **2013**, *5*, 3196-3217; d) A. Trovarelli, P. Fornasiero, *Catalysis by Ceria and Related Materials,* Imperial College Press, London, **2013**, pp. 1-888; e) T. Montini, M. Melchionna, M. Monai, P. Fornasiero, *Chem. Rev.* **2016**, *116*, 5987-6041.

[14] R. Vandenbrink, P. Mulder, R. Louw, G. Sinquin, C. Petit, J. Hindermann, *J. Catal*. **1998**, *180*, 153–160.

Entry for the Table of Contents

COMMUNICATION

Mind the gap: Europium oxybromide-based materials comprise extraordinary catalysts for both HBr oxidation to Br_2 and CH_4 oxybromination to CH_3Br, enabling a closed bromine loop for the sustainable upgrading of natural gas to fuels and chemicals.

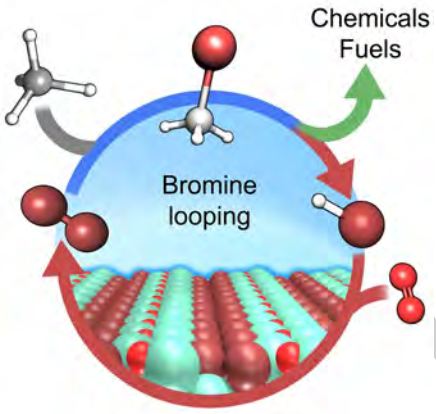

*Vladimir Paunović, Ronghe Lin, Matthias Scharfe, Amol P. Amrute, Sharon Mitchell, Roland Hauert, and Javier Pérez-Ramírez**

Page No. – Page No.
Europium Oxybromide Catalysts for Efficient Bromine Looping in Natural Gas Valorization

Supporting Information

Europium Oxybromide Catalysts for Efficient Bromine Looping in Natural Gas Valorization

Vladimir Paunović[+], Ronghe Lin[+], Matthias Scharfe, Amol P. Amrute, Sharon Mitchell, Roland Hauert, and Javier Pérez-Ramírez*

[+] Equal contribution | * Corresponding author. E-mail: jpr@chem.ethz.ch

Methods

Catalyst preparation

Commercial lanthanum(III) oxide (La_2O_3, Alfa-Aesar, 99.99%), cerium(IV) oxide (CeO_2, Sigma-Aldrich, nanopowder, 99.9%), samarium(III) oxide (Sm_2O_3, ABCR, 99.9%), europium(III) oxide (Eu_2O_3, Sigma-Aldrich, 99.5%), gadolinium(III) oxide (Gd_2O_3, Alfa-Aesar, 99.99%), terbium(III) oxide (Tb_2O_3, Stream Chemicals, 99.9%), and dysprosium(III) oxide (Dy_2O_3, ABCR, 99.99%) were heated in flowing air at 973 K for 5 h prior to the catalytic tests. Commercial titanium(IV) oxide (TiO_2, Sigma-Aldrich, rutile nanopowder, 99.5%) was heated in static air at 873 K for 5 h. Europium oxybromide (EuOBr) studied in HBr oxidation and methane oxybromination (MOB) was prepared by exposing the calcined Eu_2O_3 (2.0 g) to an HBr-containing gas-mixture (molar ratio O_2:HBr:He = 9:4.5:86.5, total flow rate F_T = 100 cm^3 min^{-1}) at 623 K (HBr oxidation) or 773 K (MOB) for 5 h. Vanadyl pyrophosphate ($(VO)_2P_2O_7$), VPO) was synthesized by refluxing a suspension of vanadium(V) oxide (V_2O_5, 15 g, Aldrich, ≥ 99.6%) in isobutanol (90 cm^3, Acros, > 99%) and benzyl alcohol (60 cm^3, Sigma-Aldrich, > 99%) for 3 h. After cooling down to room temperature, the molar P:V ratio was set to 1.2 by adding H_3PO_4 (Sigma-Aldrich, ≥ 85%) and the mixture was then refluxed for another 16 h. The blue solid was recovered by filtration, washed with isobutanol and methanol (Fluka, ≥ 99.9%), dried under vacuum (50 mbar) at 373 K for 16 h, and finally heated in flowing N_2 (Pan Gas, purity 4.5) at 873 K for 5 h. Supported Eu-based catalysts denoted as EuOBr/SiO_2, EuOBr/Al_2O_3, EuOBr/ZrO_2, EuOBr/Al_2O_3-t, and EuOBr/ZrO_2-t were prepared by impregnating an aqueous solution of $Eu(NO_3)_3{\cdot}6H_2O$ (ABCR, 99.9%) on pre-calcined (static air, 973 K, 5 h) carriers comprising SiO_2 (20-60 μm, Evonik, AEROPERL® 300/30, ≥ 99.0%), γ-Al_2O_3 (5-100 μm, Sasol, PURALOX® SCFa 140, ≥ 98%), or ZrO_2 (≤ 60 μm, Alfa-Aesar, 99%) powders and γ-Al_2O_3 (diameter: 3.2 mm, length: 3-4.5 mm, Saint-Gobain Norpro, SA6176) or ZrO_2 (diameter: 3.2 mm, length: 3-4.5 mm, Alfa-Aesar, 99%) extrudates, respectively. An appropriate amount of $Eu(NO_3)_3{\cdot}6H_2O$ was dissolved in a volume of deionized water equivalent to the pore volume of the support as determined from N_2 sorption, and the obtained solution was added dropwise to the carrier under continuous mixing. Unless otherwise stated, Eu content in supported catalysts was set to 9 wt.%. After impregnation, the material was left for 1 h at room temperature, then dried under vacuum (50 mbar) at 373 K for 12 h, and calcined in flowing air at 973 K for 5 h. Prior to evaluation, the supported catalysts were subjected to the HBr-containing gas mixture following the same protocol as for the synthesis of the bulk EuOBr. All thermal treatments were conducted using a heating rate of 5 K min^{-1}.

Catalyst characterization

Powder X-ray diffraction (XRD) was measured using a PANalytical X'Pert PRO-MPD diffractometer by applying Cu-Kα radiation (λ = 1.54060 Å). The data were recorded in the 10-70° 2θ range with an angular step size of 0.017° and a counting time of 0.26 s per step. N_2 sorption at 77 K was performed using a Micromeritics TriStar analyzer. Prior to the measurement, the sample was evacuated to 50 mbar at 573 K for 12 h. The Brunauer-Emmett-Teller (BET) method was applied to calculate the specific surface area, S_{BET}, in m^2 g^{-1}. The pore volume, V_{pore}, in cm^3 g^{-1}, was calculated from N_2 adsorption at relative pressure p/p_0 = 0.98. The content of europium in supported catalysts was

quantified by X-ray fluorescence spectroscopy (XRF), using an Orbis Micro instrument equipped with a Rh source operated at 35 kV and 500 µA. Thermogravimetric analysis (TGA) was performed using a Mettler Toledo TGA/DSC 1 Star system connected to a Pfeiffer Vacuum Thermo-Star GDS 320 T1 mass spectrometer (MS). The solid (0.05 g) was pretreated in flowing air (45 $cm^3\ min^{-1}$) at 393 K for 1 h. The analysis was carried out in the same medium (45 $cm^3\ min^{-1}$), heating at a rate of 10 K min^{-1} from 393 K to 1173 K for CeO_2 and to 1473 K for EuOBr. The evolution of bromine and water was monitored by MS, following the ions at a mass-to-charge ratio (*m*/*z*) of 81 and 18, respectively. Temperature-programmed reduction with hydrogen (H_2-TPR) was performed in a Micromeritics Autochem II 2920 unit equipped with a thermal conductivity detector (TCD). The solid (0.10 g) was loaded into a U-shaped quartz micro-reactor, pretreated in He (20 $cm^3\ min^{-1}$) at 423 K for 1 h, and cooled to 373 K. A mixture comprising 5 vol.% H_2 in N_2 (20 $cm^3\ min^{-1}$) was then fed and the temperature was increased up to 1173 K at a rate of 10 K min^{-1}, while monitoring the H_2 consumption by using a TCD detector. High-resolution transmission electron microscopy (HRTEM), high-angle annular dark field scanning transmission electron microscopy (HAADF-STEM), and elemental mapping with energy-dispersive X-ray spectroscopy (EDXS) were conducted on a FEI Talos microscope operated at 200 kV. All samples were dispersed as dry powders onto lacey carbon coated nickel grids. X-ray photoelectron spectroscopy (XPS) measurements were performed on a Physical Electronics Quantum 2000 X-ray photoelectron spectrometer using monochromatic Al-Kα radiation, generated from an electron beam operated at 15 kV, and equipped with a hemispherical capacitor electron-energy analyzer. The solids were analyzed at the electron take-off angle of 45° and the pass energy of 46.95 eV. A compensation for sample charging was obtained by referencing all the spectra to the C 1*s* at 284.5 eV. The elemental concentrations were quantified based on the measured photoelectron peak areas (Br 3*d*, Ce 3*d*, Eu 3*d*) after Shirley background subtraction using PHI-MultiPak software and the built-in relative sensitivity factors which are corrected for the system transmission function.

Catalytic evaluation

The catalytic tests were performed at ambient pressure in a continuous-flow fixed-bed reactor setup (**Figure S2**) comprising a set of (1) two-way valves and (2) digital mass-flow controllers (Bronkhorst) to feed CH_4 (PanGas, purity 5.0), HBr (Air Liquide, purity 2.8, anhydrous), O_2 (PanGas, purity 5.0), Ar (PanGas, purity 5.0; internal standard), and He (PanGas, purity 5.0; carrier gas), (3) a gas mixing unit, pressure indicator (PI), (4) a syringe pump (Nexus 6000, Chemyx) and (5) a vaporizer with a quartz T-connector filled with glass beads and operated at 343 K to supply liquid Br_2 (ABCR, 99%), (6) a homemade electrical oven accommodating (7) a quartz microreactor of 8 mm or 17 mm i.d. for tests with catalyst particles (size: 0.4-0.6 mm) or extrudates (diameter: 3.2 mm, length: 3-4.5 mm), respectively, a thermocouple (TI) fixed in a coaxial quartz thermowell with a tip positioned in the center of the (8) catalyst bed, (9) down-stream heat tracing operated at 393 K in order to prevent the condensation of unconverted reactants and reaction products, (10) a three-way sampling valves, , (11) an impinging bottle filled with KI solution (0.1 M) used to absorb Br_2 ($Br_2 + 3I^- \rightarrow I_3^- + 2Br^-$) that was quantified by iodometric titration (Mettler Toledo G20 Compact Titrator) of the formed triiodide

($I_3^- + 2S_2O_3^{2-} \rightarrow 3I^- + S_4O_6^{2-}$) with 0.01 M sodium thiosulfate solution (Aldrich, 99.99%), (12) a bed containing anhydrous Na_2CO_3 (sodium carbonate, Sigma-Aldrich, ≥ 99.5%) which was used to react with HBr ($Na_2CO_3 + 2HBr \rightarrow 2NaBr + H_2O + CO_2$), enabling quantification of its molar flow $n(HBr)^{outlet} = 2 \cdot (n(CO_2)^{bed} - n(CO_2)^{bypass})$, wherein $n(CO_2)^{bed}$ is the molar flow of CO_2 when the feed was introduced through the bed and $n(CO_2)^{bypass}$ is the molar flow of CO_2 when the feed was bypassing the bed, (13) a gas chromatograph equipped with a GS-Carbon PLOT column coupled to a mass spectrometer (GC-MS, Agilent GC 6890, Agilent MSD 5973N) enabling the on-line quantification of carbon-containing compounds (CH_4, CH_3Br, CH_2Br_2, CO, and CO_2) and Ar, and (14) impinging bottles containing aqueous NaOH solution (1 M) to neutralize the effluent gas stream. Prior to testing, the catalyst bed was heated in a He flow to the desired temperature (T = 423-793 K) and allowed to stabilize for at least 30 min before the reaction mixture was fed. The catalyst weights (W_{cat}), total flow rates (F_T), and feed applied are summarized in **Table S1**.

Each catalytic data point reported was calculated by averaging a minimum of two measurements taken after at least 1 h of stabilization under a specified condition. The conversion of HBr, X(HBr), was calculated according to Eq. 1,

$$X(\mathrm{HBr}) = \frac{\sum^{\mathrm{outlet}} N_{\mathrm{Br}}(j) \cdot n(j)^{\mathrm{outlet}}}{n(\mathrm{HBr})^{\mathrm{inlet}}} \cdot 100,\ \% \qquad \text{Eq. 1}$$

where $n(j)^{outlet}$ and $n(HBr)^{inlet}$ denote the respective molar flows of product j (j: CH_3Br, CH_2Br_2, Br_2), and HBr at the reactor outlet and inlet, and $N_{Br}(j)$ denotes the number of bromine atoms in product j. The conversion of CH_4 and CH_2Br_2, $X(i)$, (i: CH_4, CH_2Br_2) was calculated using Eq. 2,

$$X(i) = \frac{n(i)^{\mathrm{inlet}} - n(i)^{\mathrm{outlet}}}{n(i)^{\mathrm{inlet}}} \cdot 100,\ \% \qquad \text{Eq. 2}$$

where $n(i)^{inlet}$ and $n(i)^{outlet}$ are the respective molar flows of the reactant i at the reactor inlet and outlet. The selectivity to product j, $S(j)$, and the yield of product j, $Y(j)$, (j: CH_3Br, CH_2Br_2, Br_2) on the basis of HBr were determined using Eqs. 3 and 4, respectively,

$$S(j) = \frac{N_{\mathrm{Br}}(j) \cdot n(j)^{\mathrm{outlet}}}{\sum^{\mathrm{outlet}} N_{\mathrm{Br}}(j) \cdot n(j)^{\mathrm{outlet}}} \cdot 100,\ \% \qquad \text{Eq. 3}$$

$$Y(j) = \frac{X(\mathrm{HBr}) \cdot S(j)}{100},\ \% \qquad \text{Eq. 4}$$

The selectivity to product j, $S(j)$, and the yield of product j, $Y(j)$, (j: CH_3Br, CH_2Br_2, CO, CO_2) on the basis of methane were calculated using Eqs. 5 and 6, respectively,

$$S(j) = \frac{n(j)^{\mathrm{outlet}}}{\sum^{\mathrm{outlet}} n(j)^{\mathrm{outlet}}} \cdot 100,\ \% \qquad \text{Eq. 5}$$

$$Y(j) = \frac{X(i) \cdot S(j)}{100}, \%$$ Eq. 6

The errors of the bromine mass balance, ε_{Br}, and carbon mass balance, ε_C, were determined using Eqs. 7 and 8, respectively,

$$\varepsilon_{Br} = \frac{n(\mathrm{HBr})^{\mathrm{inlet}} - \left(n(\mathrm{HBr})^{\mathrm{outlet}} + \sum^{\mathrm{outlet}} N_{\mathrm{Br}}(j) \cdot n(j)^{\mathrm{outlet}} \right)}{n(\mathrm{HBr})^{\mathrm{inlet}}} \cdot 100, \%$$ Eq. 7

$$\varepsilon_C = \frac{\sum^{\mathrm{inlet}} n(i)^{\mathrm{inlet}} - \left(n(\mathrm{CH_4})^{\mathrm{outlet}} + \sum^{\mathrm{outlet}} n(j)^{\mathrm{outlet}} \right)}{\sum^{\mathrm{inlet}} n(i)^{\mathrm{inlet}}} \cdot 100, \%$$ Eq. 8

In all experiments, the errors of the bromine and carbon mass balance were less than 5%. After the tests, the reactor was quenched to room temperature in He flow and the catalyst was retrieved for *ex situ* characterization.

Table S1. Catalyst weights, total flow rates, and feed compositions applied in the reactions studied.

Reaction	W_{cat} / g	F_T / $cm^3\ min^{-1}$	Feed composition[a] / mol.%				
			CH_4	CH_2Br_2	HBr	Br_2	O_2
HBr oxidation	0.5 (2.0)[b]	100	0	0	4.5 (10)[b]	0	1.13-9
CH_4 oxybromination	1.0 (0.5)[b,c]	50-200	3-19	0	3-12	0	1.5-6
CH_4 bromination	1.0[c]	100	6	0	0	3	0
CH_4 oxidation	1.0	100	6	0	0	0	3
CH_2Br_2 oxidation	1.0	100	0	1	3	0	1

[a] Ar (4.5 mol.%) was added as an internal standard to all the reaction mixtures, except those applied in HBr oxidation. He was used as the balance gas.

[b] Values in brackets refer to tests over catalyst extrudates.

[c] In the oxybromination and bromination of methane, the catalyst was mixed with inert quartz particles (size: 0.15-0.3 mm) to ensure a constant bed volume (V_{bed} = 2 cm^3).

Table S2. Specific surface areas (S_{BET}) of the bulk catalysts in their fresh form and after the HBr oxidation and methane oxybromination (MOB) tests (used) shown in **Figure S4**, and **Figures 2a**,**3** of the main manuscript.

Catalyst[a]	S_{BET} / $m^2\ g^{-1}$	
	fresh	used
HBr oxidation		
EuOBr	22	19
CeO_2	27	26
LaOBr	2	4
SmOBr	1	2
DyOBr	2	8
GdOBr	1	10
TbOBr	6	4
TiO_2	18	16
MOB		
EuOBr	6	6
CeO_2	22	20
VPO	28	22

[a] The pore volume of the bulk catalysts was lower than 0.14 $cm^3\ g^{-1}$.

Table S3. Specific surface areas (S_{BET}) and pore volumes (V_{pore}) of the supported Eu-based catalysts in their fresh form and after the HBr oxidation and methane oxybromination (MOB) tests shown in **Figures 3**,**4** of the main manuscript.

Catalyst	S_{BET} / m^2 g^{-1}			V_{pore} / cm^3 g^{-1}		
	fresh	HBr oxidation	MOB	fresh	HBr oxidation	MOB
$EuOBr/Al_2O_3$	127	114	92	0.42	0.38	0.37
$EuOBr/Al_2O_3$-t	235	187	-	0.72	0.68	-
$EuOBr/ZrO_2$	29	25	24	0.19	0.16	0.14
$EuOBr/ZrO_2$-t	55	-	51	0.21	-	0.24
$EuOBr/SiO_2$	204	195	190	1	0.85	0.80

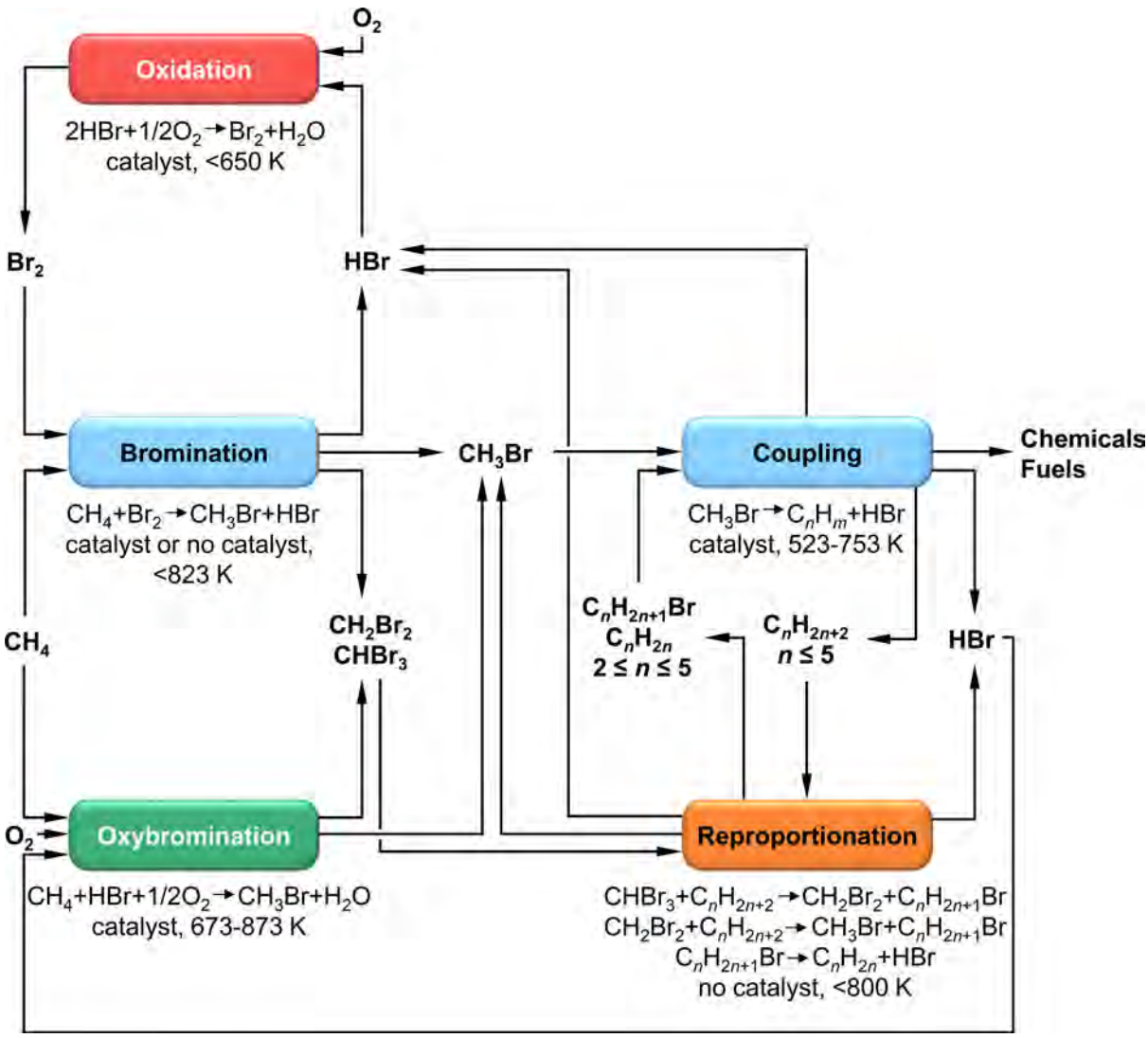

Figure S1. Process flow diagram of bromine-mediated natural gas upgrading. The activation of methane typically starts with its non-catalytic gas-phase bromination (left, middle) (Zhou *et al.,* US-B1 6472572, **2002**; Waycuilis, US-B2 7244867, **2007**; Gadewar *et al.*, US-A1 2010/0096588, **2010**; Waycuilis, Turner, US-A1 2013/0102820, **2013**). The coupling of CH_3Br (right, middle) over zeolite catalysts yields various hydrocarbons (C_nH_m) such as gasolines, olefins, and aromatics (Waycuilis, US-B2 7244867, **2007**; Gadewar *et al.*, US-A1 2010/0096588, **2010**; Zhang *et al., Phys. Chem. Chem. Phys.* **2011**, *13*, 2550-2555; He *et al.*, *Angew. Chem. Int. Ed.* **2012**, *51*, 2438-2442; *Angew. Chem.* **2012**, *124*, 2488-2492; Waycuilis, Turner, US-A1 2013/0102820, **2013**). Polybrominated byproducts of methane bromination comprising dibromomethane (CH_2Br_2) and trace amounts of tribromomethane ($CHBr_3$) can promote coking in zeolite catalysts (Lin *et al.*, Chem. Rev. **2017**, *172*, 4182-4247) and are commonly reproportionated (right, bottom) with alkanes (C_nH_{2n+2}) obtained in CH_3Br coupling ($n \leq 5$) or contained in natural gas ($n \leq 4$) (Lorkovic *et al.*, *J. Phys. Chem. A* **2006**, *110*, 8695−8700; Gadewar *et al.*, US-A1 2010/0096588, **2010**; Fong, Swain, US-A1 2010/0234637, **2010**; Waycuilis, Turner, US-A1 2013/0102820, **2013**) yielding CH_3Br, brominated alkanes ($C_nH_{2n+1}Br$), and olefins (C_nH_{2n}) that can be valorized via coupling.

Recycling of hydrogen bromide HBr, which is a stoichiometric byproduct of both methane bromination and methyl bromide coupling, closes the bromine loop. This is vital for the feasibility of bromine-

mediated routes for natural gas upgrading because of the high price and low availability of this halogen. Catalytic HBr oxidation recovers molecular bromine (left, top) enabling continuous bromine looping (Moser *et al.*, *ChemCatChem* **2013**, *5*, 3520-3523; Moser, *Angew. Chem. Int. Ed*. **2014**, *53*, 8628-8633; *Angew. Chem.* **2014**, *126*, 8772-8777). HBr can also be recycled through catalytic oxybromination (left, bottom) by the direct reaction with methane and oxygen to yield CH_3Br (He *et al.*, *Angew. Chem. Int. Ed.* **2012**, *51*, 2438-2442; *Angew. Chem.* **2012**, *124*, 2488-2492; Paunovic *et. al.*, *Nat. Chem.* **2016**, 8, 803-809; Lin *et al.*, Chem. Rev. **2017**, *172*, 4182-4247), offering a highly attractive route for process intensification. A key challenge for oxybromination with respect to the two-step HBr oxidation and methane bromination is to avoid the formation of carbon oxides (CO_x) due to the combustion of methane and/or brominated products in the presence of oxygen.

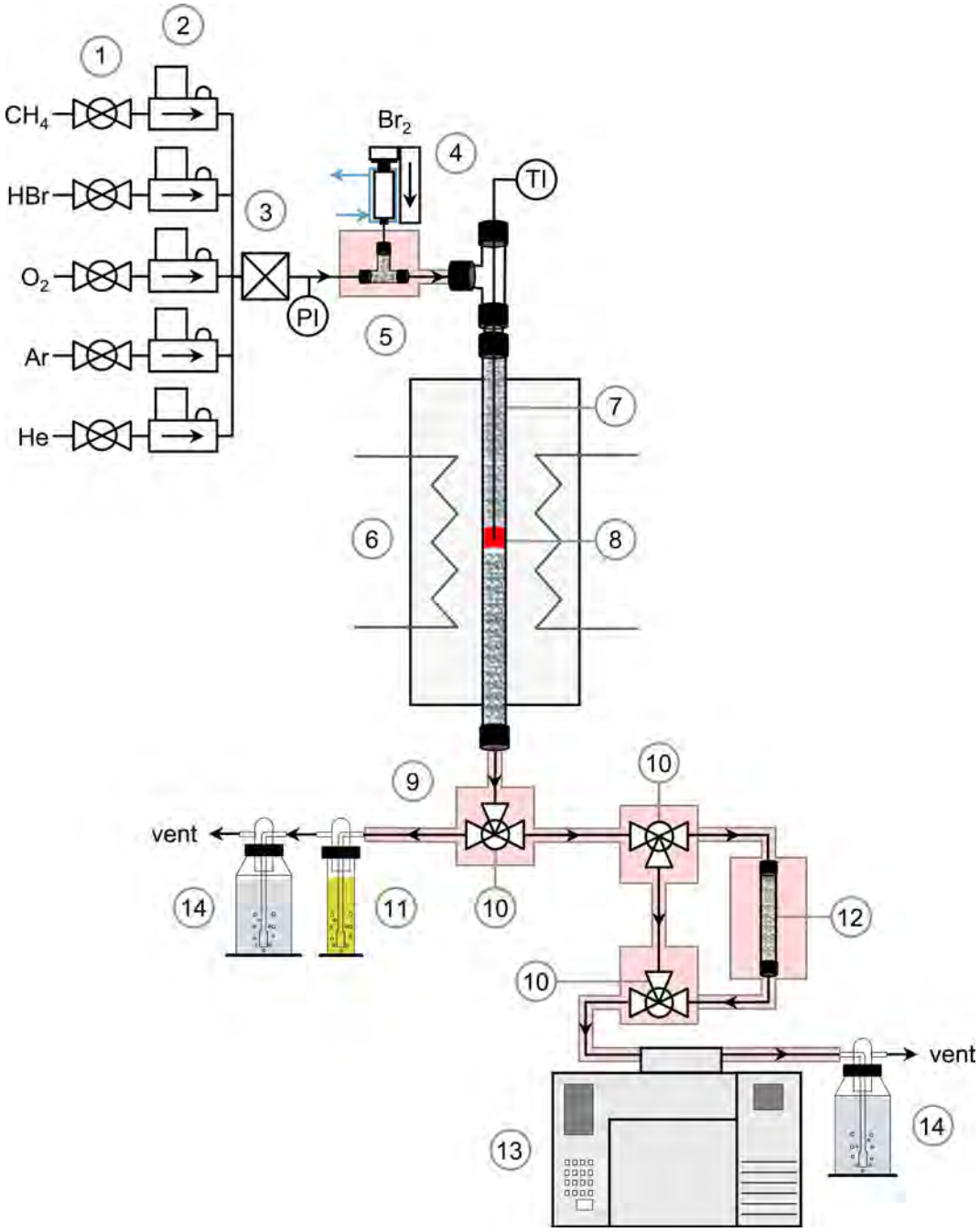

Figure S2. Flowsheet of the laboratory setup used for the continuous-flow HBr oxidation, methane oxybromination, methane bromination, and methane oxidation reactions. 1: two-way on-off valves, 2: mass flow controllers, 3: gas mixer, 4: syringe pump with water-cooling system, 5: vaporizer, 6: oven, 7: quartz reactor, 8: catalyst bed, 9: heat tracing (pink), 10: three-way sampling valves, 11: KI impinging bottle, 12: Na_2CO_3 bed, 13: GC-MS, 14: NaOH impinging bottle, PI: pressure indicator, and TI: temperature indicator.

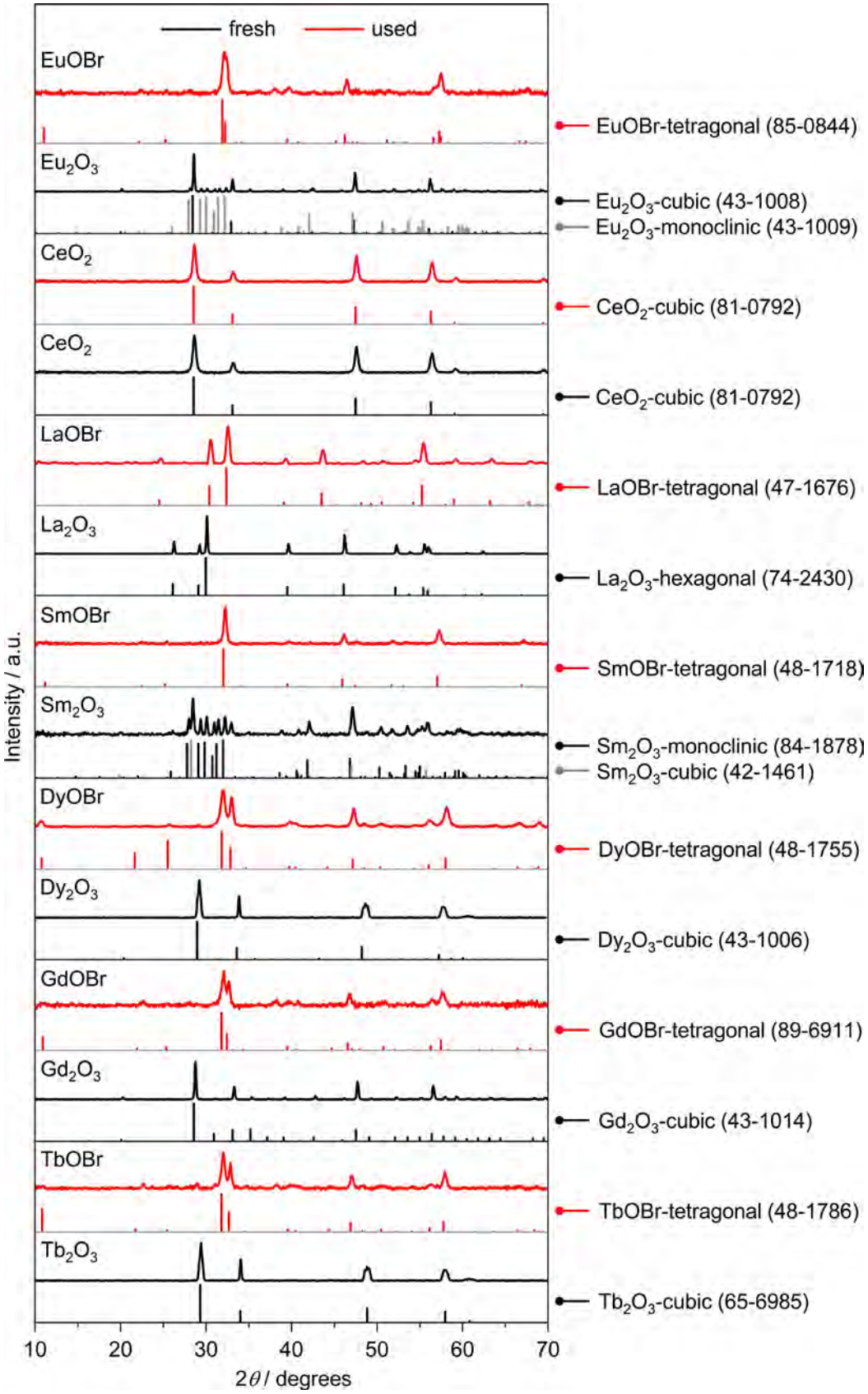

Figure S3. X-ray diffractograms of the catalysts applied in the HBr oxidation tests shown in **Figure S4** in fresh (black) and used (red) forms. Reference patterns shown as vertical lines below the measured diffractograms are identified on the right with their ICDD-PDF numbers.

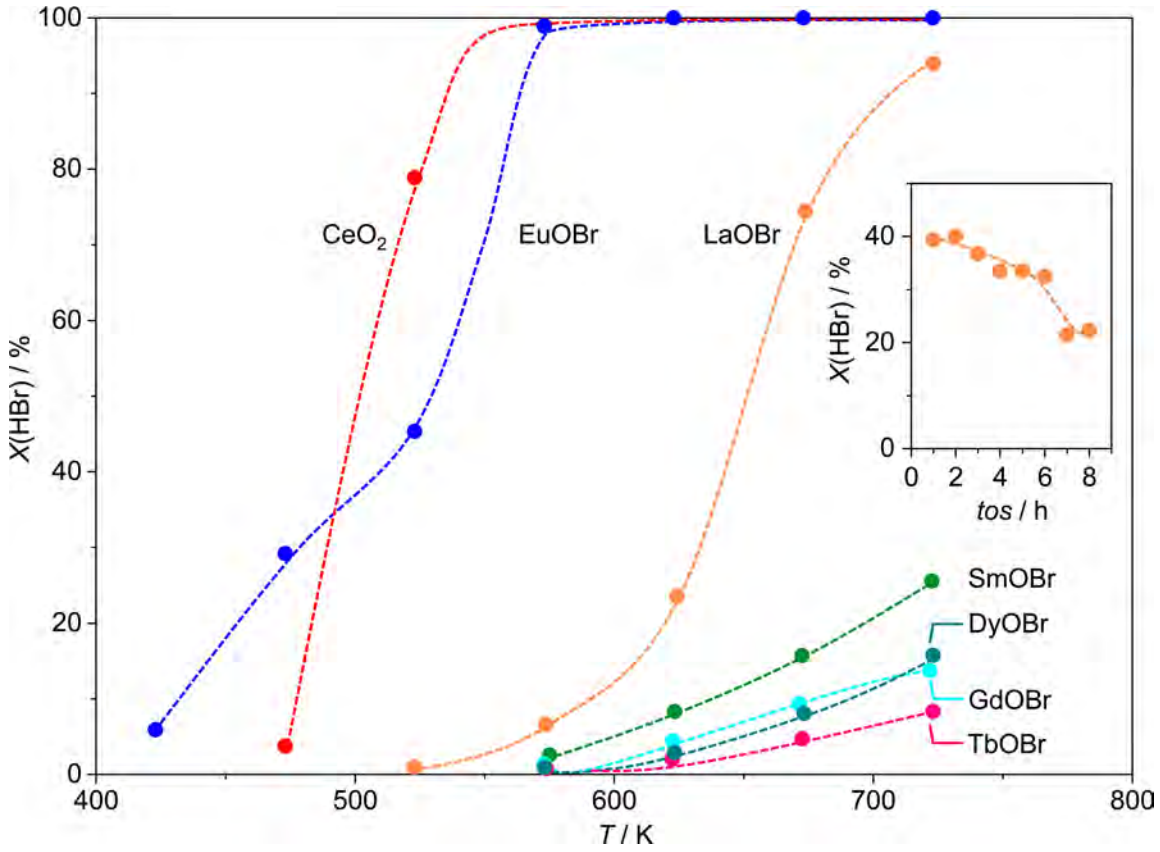

Figure S4. Catalytic performance of different lanthanide oxides and oxybromides in HBr oxidation. Conditions: HBr:O_2:He = 4.5:9:86.5, F_T/W_{cat} = 200 cm^3 min^{-1} g_{cat}^{-1}, P = 1 bar. The tests were performed using an oxide as starting material and ramping from the highest to the lowest temperature. XRD analysis of the used samples (**Figure S3**) revealed that all the oxides were transformed into the corresponding oxybromides, with the exception of CeO_2 which preserved the bulk oxide structure. The catalysts were thus named according to the dominant phase identified by XRD in the materials recovered after the temperature ramp, which is anticipated to be the active phase. Among the tested catalysts, EuOBr showed exceptionally high activity, exceeding that of the benchmark CeO_2 at low temperatures. The light-off curve of LaOBr was shifted to *ca*. 150 K higher temperature compared to EuOBr, while other oxybromides exhibited little activity in the preferred temperature window (≤ 573 K). The specific surface areas of these catalysts are ca. 2-10 times lower compared to EuOBr (**Table S2**). Still, their initial activity (≤ 573 K) is ca. 20-100 times lower compared to the latter catalyst, indicating that the exceptional performance of EuOBr is not only the consequence of its higher surface area. It is interesting to note that some of the used materials (LaOBr, SmOBr, DyOBr, GdOBr) showed an increased surface area with respect to the fresh materials (**Table S2**), suggesting the occurrence of restructuring on transformation from the oxide to the oxybromide phase. A short time-on-stream (*tos*) tests (HBr:O_2:He = 4.5:9:86.5, F_T/W_{cat} = 200 cm^3 min^{-1} g_{cat}^{-1}, P = 1 bar, T = 523 K (EuOBr, CeO_2), 673 K (LaOBr), 723 K (SmOBr, DyOBr, GdOBr, TbOBr), *tos* = 8 h) demonstrated stable catalytic performance of all the catalysts, except LaOBr (**Figure S4**, inset). The activity of the latter was substantially reduced after 8 h, indicative of catalyst instability even under oxygen-rich conditions (O_2:HBr = 2, *i.e.* fourfold oxygen excess with respect to the stoichiometric O_2:HBr = 0.25).

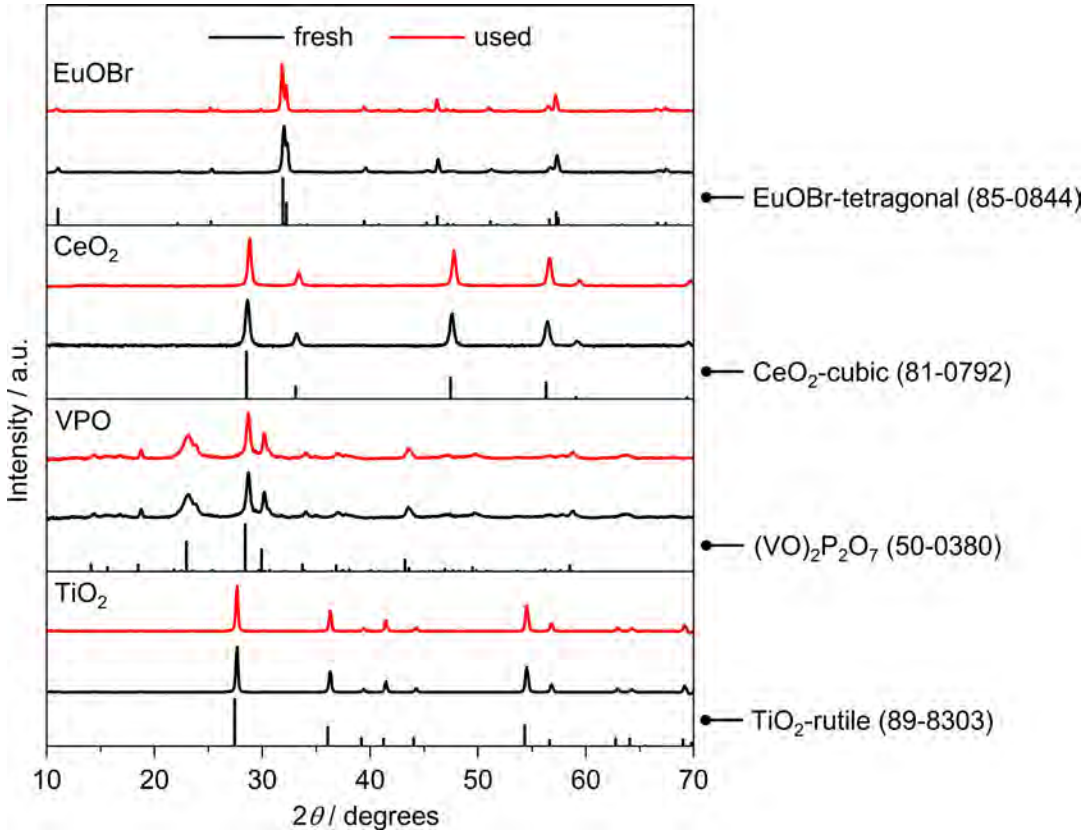

Figure S5. X-ray diffractograms of the TiO_2 catalyst applied in the HBr oxidation test and of the EuOBr, CeO_2, and VPO catalysts applied in the MOB tests shown in **Figures 2a**,**3** of the main manuscript, respectively, in fresh (black) and used (red) form. Reference patterns shown as vertical lines below the measured diffractograms are identified on the right with their ICDD-PDF numbers.

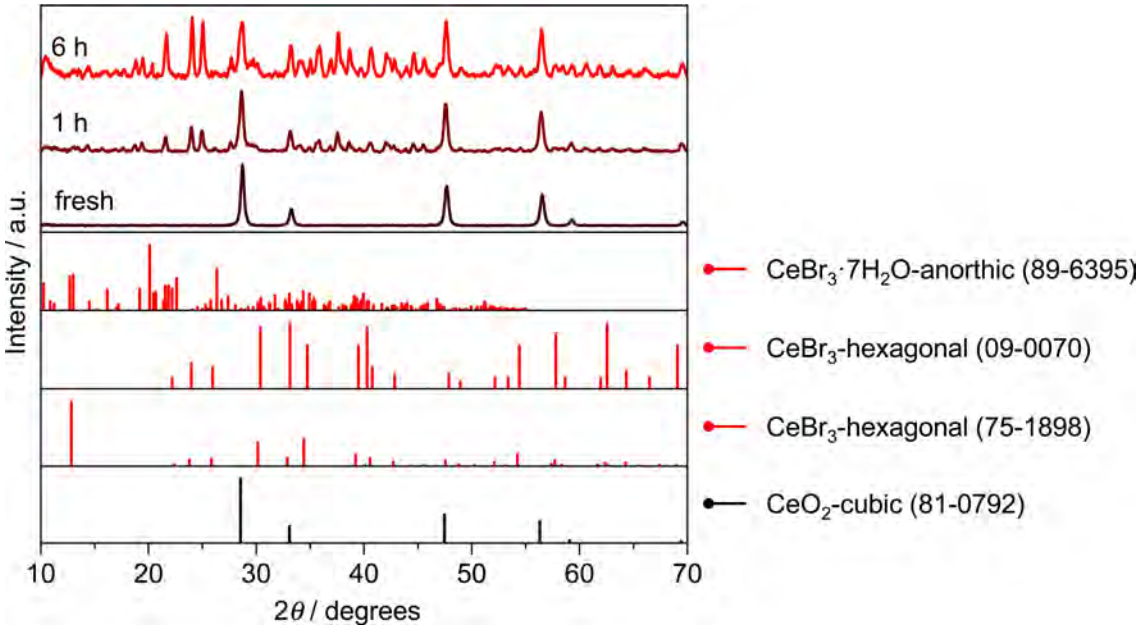

Figure S6. X-ray diffractograms of the CeO_2 catalysts in their fresh form and recovered after different time-on-stream in HBr oxidation. Conditions: HBr:O_2:He = 4.5:1.13:94.37, F_T/W_{cat} = 200 $cm^3\ min^{-1}\ g_{cat}^{-1}$, T = 523 K, P = 1 bar. X-ray diffractograms of the CeO_2 catalysts in their fresh form and recovered after different time-on-stream in HBr oxidation. The results of the microscopy (**Figure S7**) and thermogravimetric (**Figure S8**) analysis suggest the formation of new (oxy)bromide phases(s) of cerium during the reaction. This is also substantiated by the appearance of new peaks in the diffractograms of the used catalysts, which however did not match the reflections of any previously reported oxides or bromides of ceria.

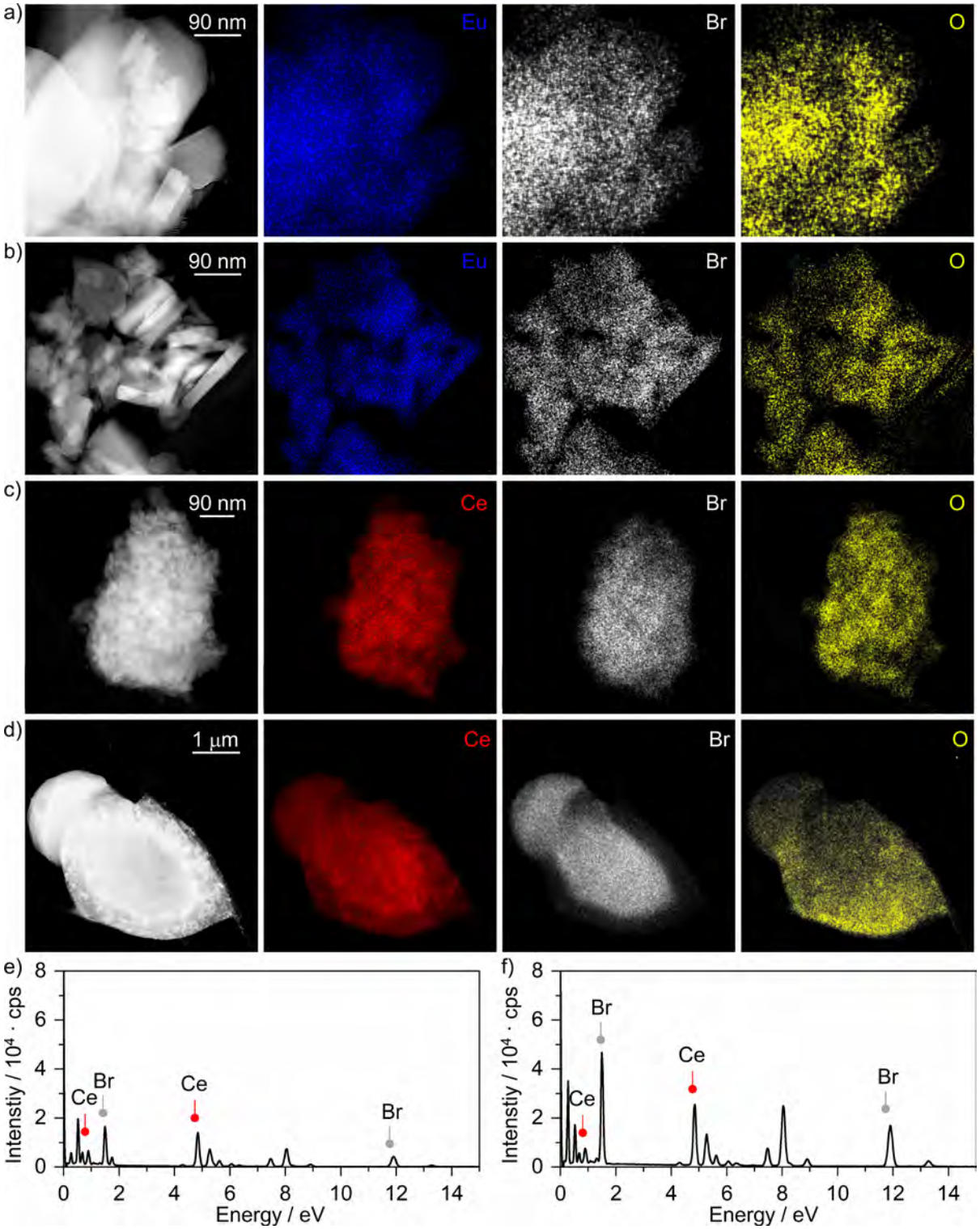

Figure S7. HAADF-STEM micrographs (left) and electron dispersive X-ray spectroscopy elemental maps (right) of EuOBr in a) fresh form and b) recovered after 20 h on-stream, and CeO_2 recovered after c) 1 h and d) 6 h on-stream. Electron dispersive X-ray spectra of CeO_2 recovered after e) 1 h and f) 6 h on stream. Conditions: HBr:O_2:He = 4.5:1.13:94.37, F_T/W_{cat} = 200 cm^3 min^{-1} g_{cat}^{-1}, T = 523 K, P = 1 bar. HAADF-STEM micrographs of EuOBr indicate that rod-like morphology and particle size of EuOBr are preserved under hash reaction conditions, while elemental maps testify the uniform distribution of europium, bromine, and oxygen in fresh and used catalysts (**Figure S7a**,**b**). In

contrast to this, CeO_2 undergoes substantial particle agglomeration (**Figure S7c**,**d**, left) in line with a drop in surface area. The catalyst exhibits a significant bromine uptake already after 1 h of operation (**Figure S7c**), which is continuously increasing during reaction as inferred from the relative ratio of Br and Ce peaks in X-ray spectra of 1 h and 6 h samples (**Figure S7e**,**f**), as well as thermogravimetric analysis (**Figure S8**).Thereby, the catalyst recovered after 6 h on-stream shows significant depletion of oxygen and enrichment in bromine (**Figure S7d**), which along with particle agglomeration leads to the fast deactivation of CeO_2 (**Figure 2c** of the main manuscript).

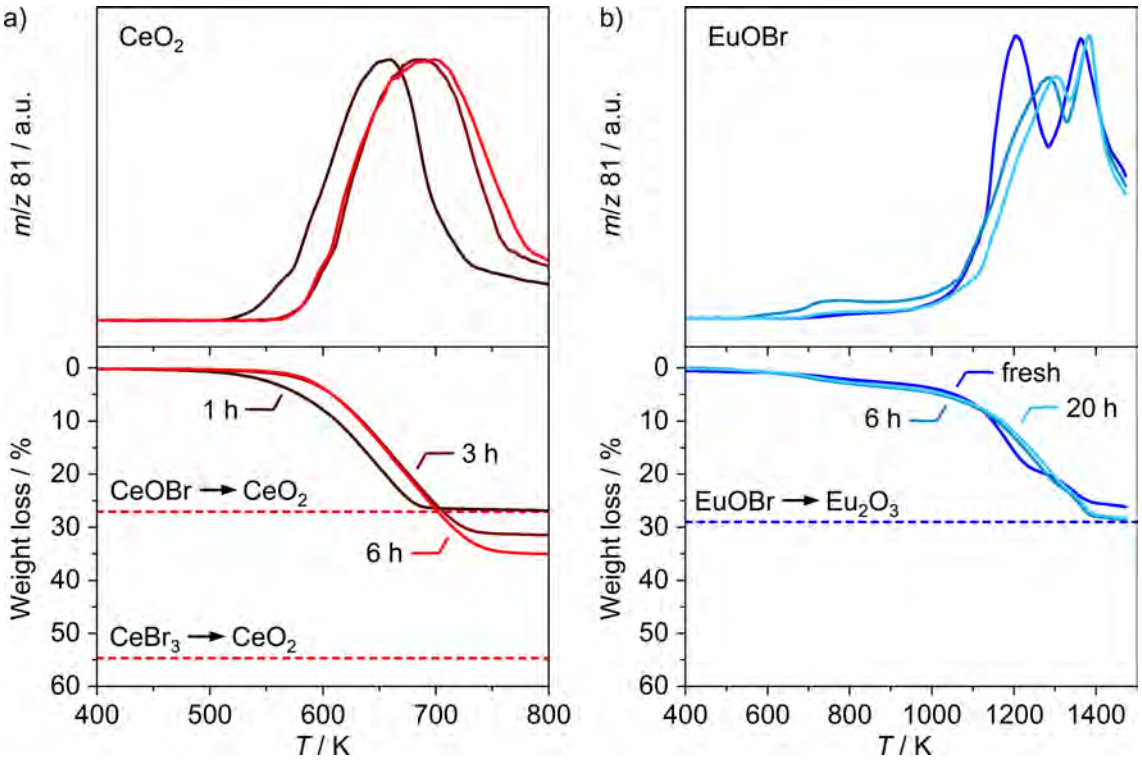

Figure S8. Thermogravimetric analysis (TGA) and the Br_2 evolution signals over a) CeO_2 and b) EuOBr prior to (fresh) and after *n* hours of HBr oxidation under a stoichiometric feed. Conditions: HBr:O_2:He = 4.5:1.13:94.37, F_T/W_{cat} = 200 cm^3 min^{-1} g_{cat}^{-1}, T = 523 K, P = 1 bar. Dashed lines indicate the theoretical weight loss for the transformations indicated. Shaded areas highlight the typical operating window of HBr oxidation and methane oxybromination. The weight loss of used CeO_2 demonstrates a time-progressive bromination of the catalyst, which results in a drop in the HBr conversion (**Figure 2c** of the main article), suggesting an inherently low activity of the brominated ceria phases. In stark contrast to this, EuOBr exhibits a high activity in HBr oxidation, and high resistance to further bromination, as also corroborated by the identical TGA profiles of the catalysts after 6 h and 20 h on stream, the weight loss of which agrees with the theoretical value (29%) for the transformation of EuOBr into Eu_2O_3. The difference between the fresh and used samples likely results from the incomplete conversion to EuOBr during the pretreatment period, but has no impact on the catalyst activity. Note that even under the HBr-free feed in which TGA was performed, the transformation of EuOBr into Eu_2O_3 occurs at temperatures exceeding those applied in HBr oxidation and MOB, confirming the stability of this phase against reoxidation.

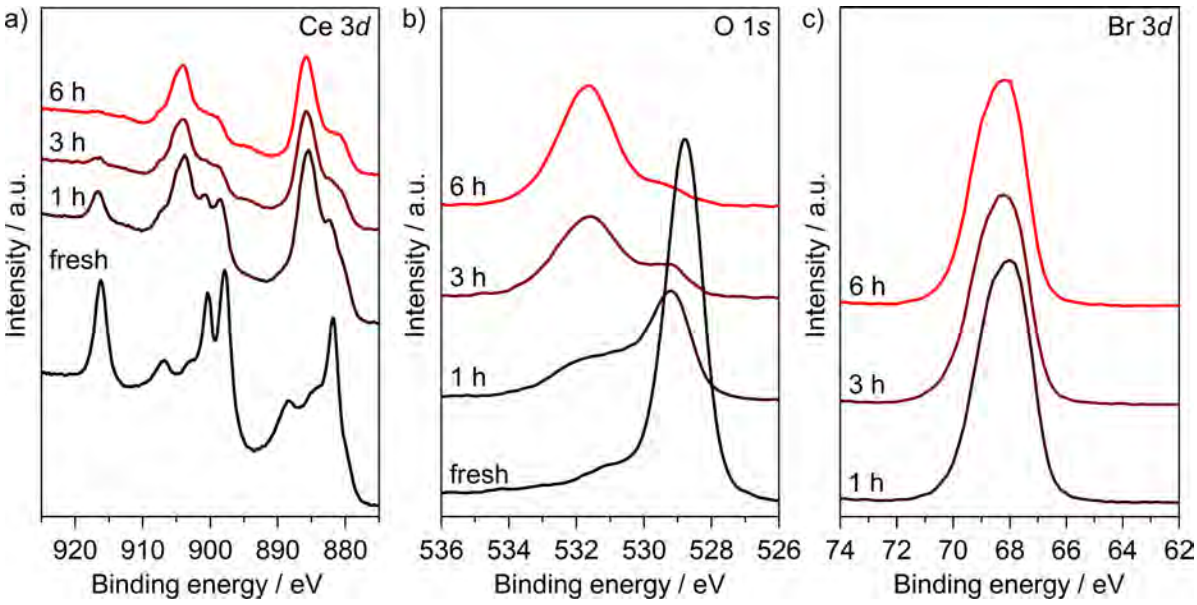

Figure S9. a) Ce 3*d*, b) O 1*s*, and c) Br 3*d* X-ray core level spectra of CeO_2 prior to (fresh) and after *n* hours of HBr oxidation under a stoichiometric feed. Conditions: HBr:O_2:He = 4.5:1.13:94.37, F_T/W_{cat} = 200 $cm^3\ min^{-1}\ g_{cat}^{-1}$, T = 523 K, P = 1 bar. The Ce 3*d* spectrum of fresh CeO_2 comprises three pairs of spin-orbit doublets indicating that Ce is present in the oxidation state Ce^{4+}, while the used samples after 3 h show only two pairs of doublets, typical of Ce^{3+}. These spectra are fully consistent with those reported in the literature (Mullins *et al.*, *Surf. Sci*. **1998**, *409*, 307-319), testifying the reduction of Ce^{4+} into Ce^{3+} upon bromination. A shift of the O 1*s* peak in fresh CeO_2 (529 eV) to higher binding energy (531.8 eV) in used samples likely originates from the protonation of oxygen atoms (Ai *et al.*, *Environ. Sci. Technol*. **2009**, *43*, 4143-4150).

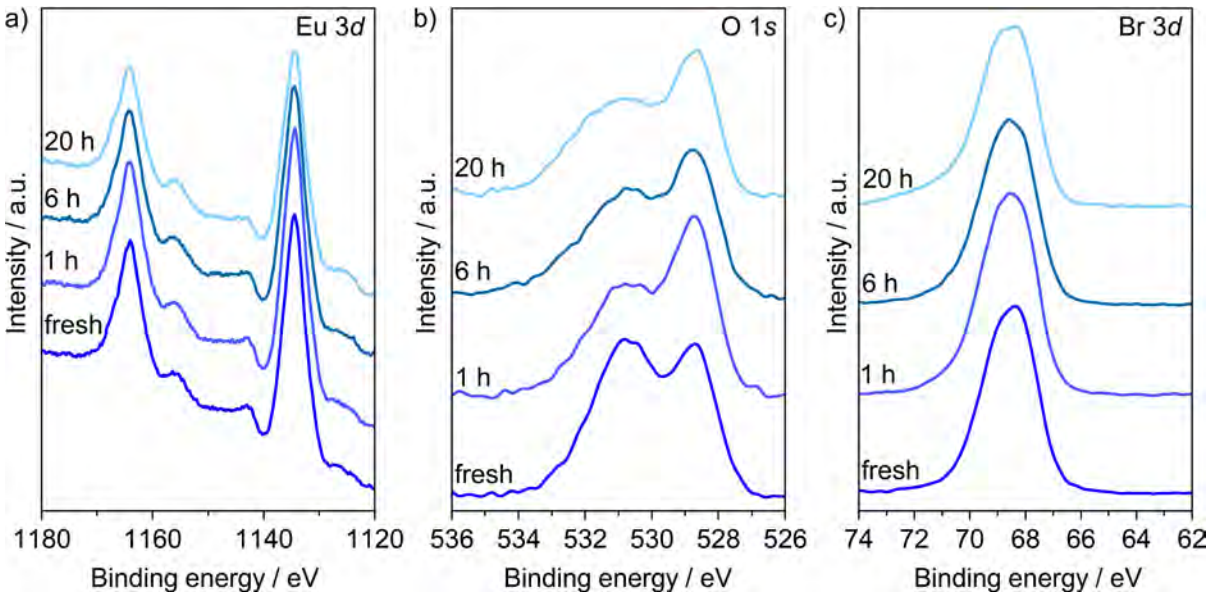

Figure S10. a) Eu 3*d*, b) O 1*s*, and c) Br 3*d* X-ray core level spectra of EuOBr prior to (fresh) and after *n* hours of HBr oxidation under a stoichiometric feed. Conditions: $HBr:O_2:He = 4.5:1.13:94.37$, $F_T/W_{cat} = 200\ cm^3\ min^{-1}\ g_{cat}^{-1}$, $T = 523$ K, $P = 1$ bar. The Eu 3*d* core level spectra displays dominant peaks at binding energies of 1134 eV ($3d_{5/2}$) and 1164 eV ($3d_{3/2}$), which are ascribed to Eu^{3+}, with small contributions at 1128 eV ($3d_{5/2}$) and 1156 eV ($3d_{3/2}$), corresponding to Eu^{2+} (Pol *et al.*, *Chem. Mater.* **2002**, *14*, 3920-3924). In contrast to CeO_2 (**Figure S9**), no signs of catalyst reduction could be observed, as the ratio of Eu^{2+}/Eu^{3+} remains unaltered. O 1*s* spectra exhibit two peaks at 528.9 eV and 531.8 eV, which can be ascribed to oxide-like species and oxygen atoms that are close to electronegative bromine atoms, respectively (Mercier *et al.*, *J. Electron. Spectrosc.* **2006**, *150*, 21-26). Note that, after initial stabilization the shape of the O 1*s* spectra is essentially constant for the catalysts used for 1 , 6 h, and 20 h, further corroborating the stability of the catalyst surface under the stoichiometric feed composition.

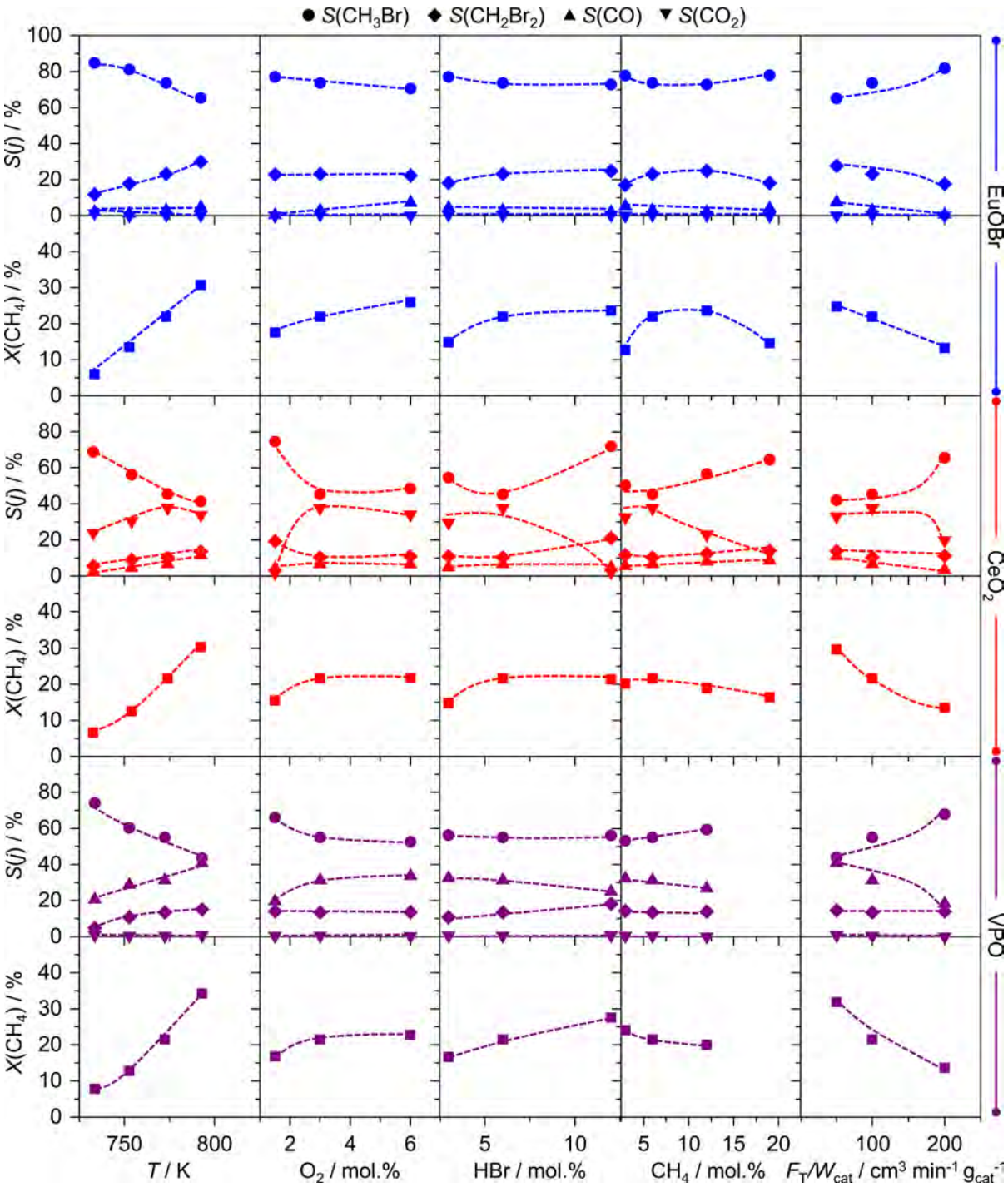

Figure S11. Conversion of methane, $X(CH_4)$, and product selectivity on the basis of methane, $S(j)$, in MOB *versus* temperature (CH_4:HBr:O_2:Ar:He = 6:6:3:4.5:80.5, F_T/W_{cat} = 100 cm^3 min^{-1} g$_{cat}^{-1}$), oxygen concentration (CH_4:HBr:O_2:Ar:He = 6:6:1.5-6:4.5:82-77.5, F_T/W_{cat} = 100 cm^3 min^{-1} g$_{cat}^{-1}$, T = 773 K), HBr concentration (CH_4:HBr:O_2:Ar:He = 6:3-12:3:4.5:83.5-74.5, F_T/W_{cat} = 100 cm^3 min^{-1} g$_{cat}^{-1}$, T = 773 K), methane concentration (CH_4:HBr:O_2:Ar:He = 3-19:6:3:4.5:80.5-73.5, F_T/W_{cat} = 100 cm^3 min^{-1} g$_{cat}^{-1}$, T = 773 K), and space velocity (CH_4:HBr:O_2:Ar:He = 6:6:3:4.5:80.5, F_T/W_{cat} = 50-200 cm^3 min^{-1} g$_{cat}^{-1}$, T = 773 K) over EuOBr, CeO_2, and VPO at P = 1 bar.

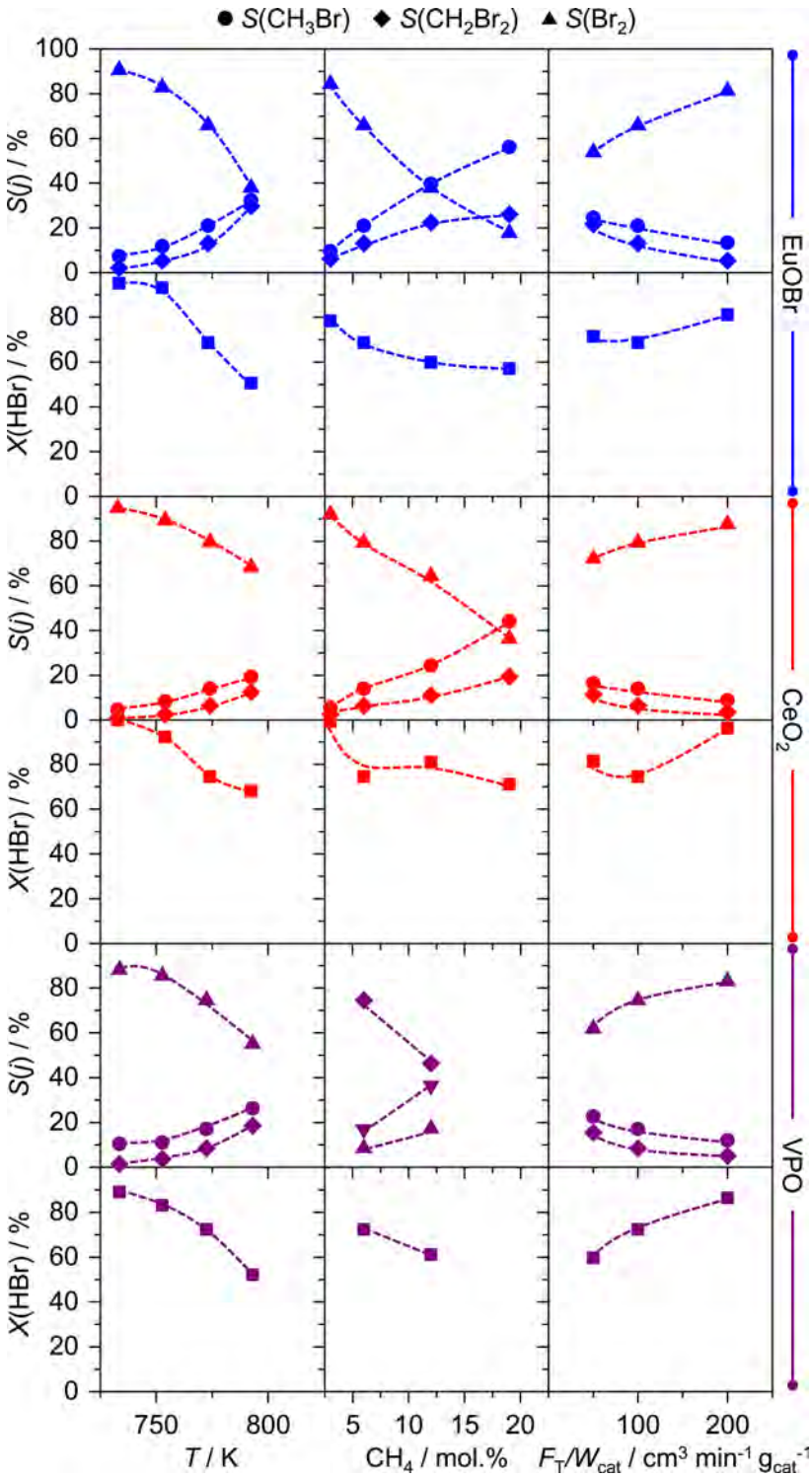

Figure S12. Conversion of HBr, *X*(HBr), and product selectivity on the basis of HBr, *S*(*j*), in MOB *versus* temperature (CH_4:HBr:O_2:Ar:He = 6:6:3:4.5:80.5, F_T/W_{cat} = 100 cm^3 min^{-1} g_{cat}^{-1}), methane concentration (CH_4:HBr:O_2:Ar:He = 3-19:6:3:4.5:80.5-73.5, F_T/W_{cat} = 100 cm^3 min^{-1} g_{cat}^{-1}, *T* = 773 K), and space velocity (CH_4:HBr:O_2:Ar:He = 6:6:3:4.5:80.5, F_T/W_{cat} = 50-200 cm^3 min^{-1} g_{cat}^{-1}, *T* = 773 K) over EuOBr, CeO_2, and VPO at *P* = 1 bar.

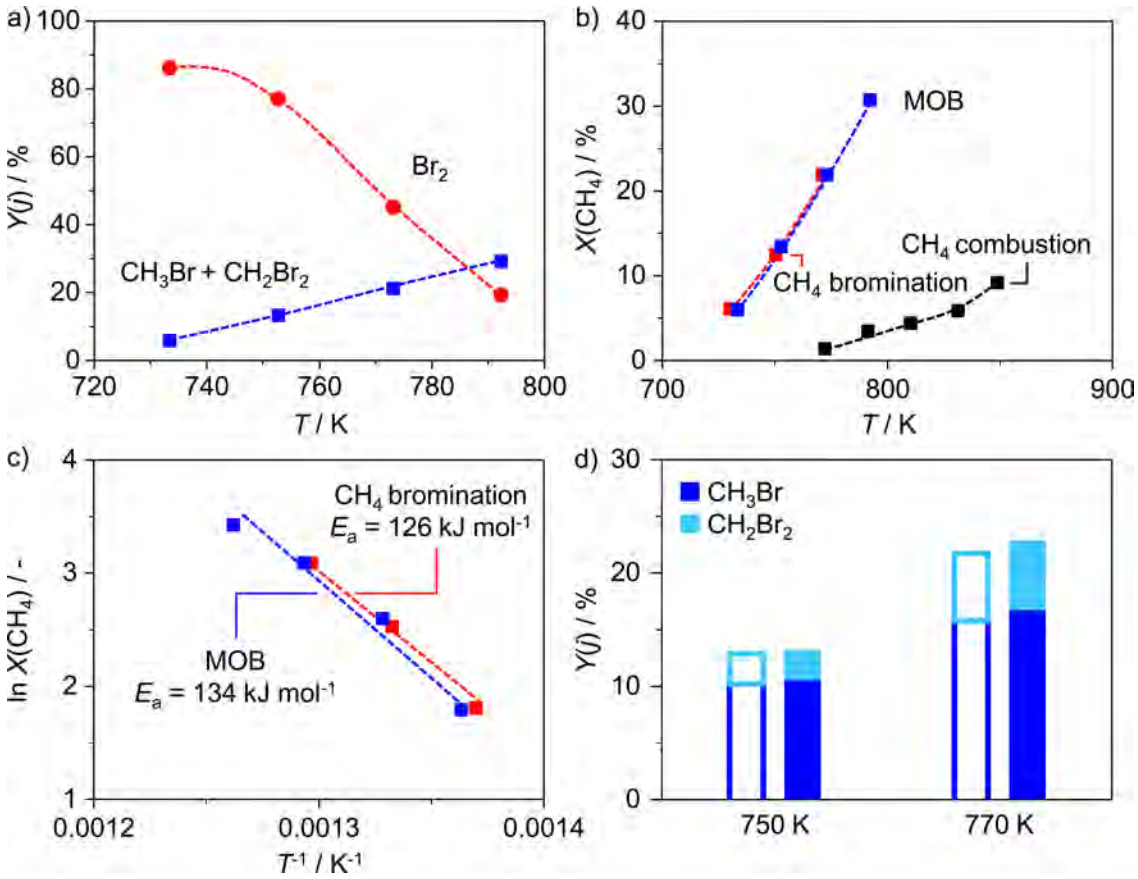

Figure S13. a) Yield, *Y*(*j*), of bromine on the basis of HBr and bromomethanes (CH_3Br+CH_2Br_2) on the basis of CH_4 *versus* temperature in MOB over EuOBr. b) Conversion of methane *versus* temperature in MOB and methane combustion ($CH_4 + (x/2+1)O_2 \rightarrow CO_x + 2H_2O$) over EuOBr, and methane bromination ($CH_4 + xBr_2 \rightarrow CH_{(4-x)}Br_x + xHBr$) over quartz. c) Arrhenius plots used to derive the apparent activation energies, E_a, for MOB over EuOBr and for methane bromination over quartz. d) Yield of bromomethanes in methane bromination at two different temperatures over quartz (open bars) and EuOBr (solid bars). MOB (CH_4:HBr:O_2:Ar:He = 6:6:3:4.5:80.5), methane combustion (CH_4:O_2:Ar:He = 6:3:4.5:86.5), and methane bromination (CH_4:Br_2:Ar:He = 6:3:4.5:86.5) were performed at F_T/W_{cat} = 100 $cm^3\ min^{-1}\ g_{cat}^{-1}$ and P = 1 bar. Bromine is the main product in MOB over EuOBr at lower reaction temperatures (*ca.* 730 K), which only yields low amounts of bromomethanes (**Figure S12**,**S13a**). An increased production of bromomethanes upon increasing the reaction temperature (750-795 K) is coupled to a drop in the bromine yield (**Figure S13a)** and HBr conversion (**Figure S12**). Selectivity to bromine and HBr conversion also decrease with an increase in methane concentration and a decrease in space-velocity, which favor the generation of bromomethanes (**Figure S12**), suggesting that their formation might proceed by the reaction of methane with the molecular bromine generated by heterogenous HBr oxidation. Moreover, the temperature region of MOB overlaps with that of the non-catalytic bromination of methane over quartz particles (**Figure S13b**) and the reactions have similar apparent activation energies (**Figure S13c**). To elucidate the role of EuOBr in methane activation under MOB conditions, methane combustion was studied over this catalyst using identical CH_4:O_2 ratio as the one applied in MOB (**Figure S13b**). The much lower conversion of methane in the combustion reaction compared to MOB indicates the low propensity of EuOBr to activate C-H bonds in the temperature window of MOB. This is further

corroborated by conducting methane bromination over EuOBr and comparing the performance with the reaction over quartz particles (**Figure S13d**). The two tests provided almost identical yields of bromomethanes, demonstrating that EuOBr has no particular advantage for methane activation by bromine with respect to quartz. These results hint that the gas-phase reaction of methane with bromine generated by catalytic HBr oxidation is likely the dominant pathway for C-Br bond formation in MOB over EuOBr.

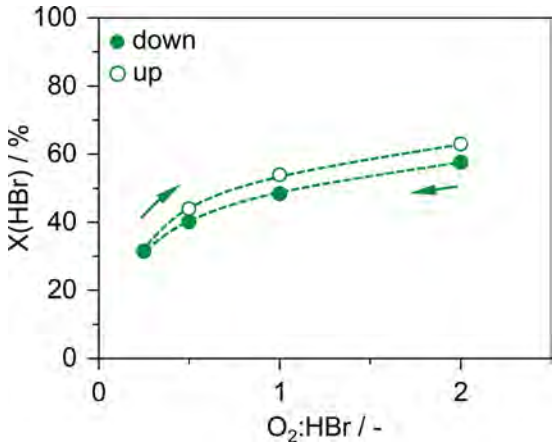

Figure S14. Conversion of HBr *versus* the molar O_2:HBr ratio over. $EuOBr/Al_2O_3$. Conditions: HBr:O_2:He = 4.5:1.13-9:94.37-86.5, F_T/W_{cat} = 200 $cm^3\ min^{-1}\ g_{cat}^{-1}$, T = 523 K, P = 1 bar. The oxygen content was changed from the highest to the lowest value (down) and then increased back to the starting point (up). The test demonstrates that the robustness of bulk EuOBr is preserved in the supported catalytic system.

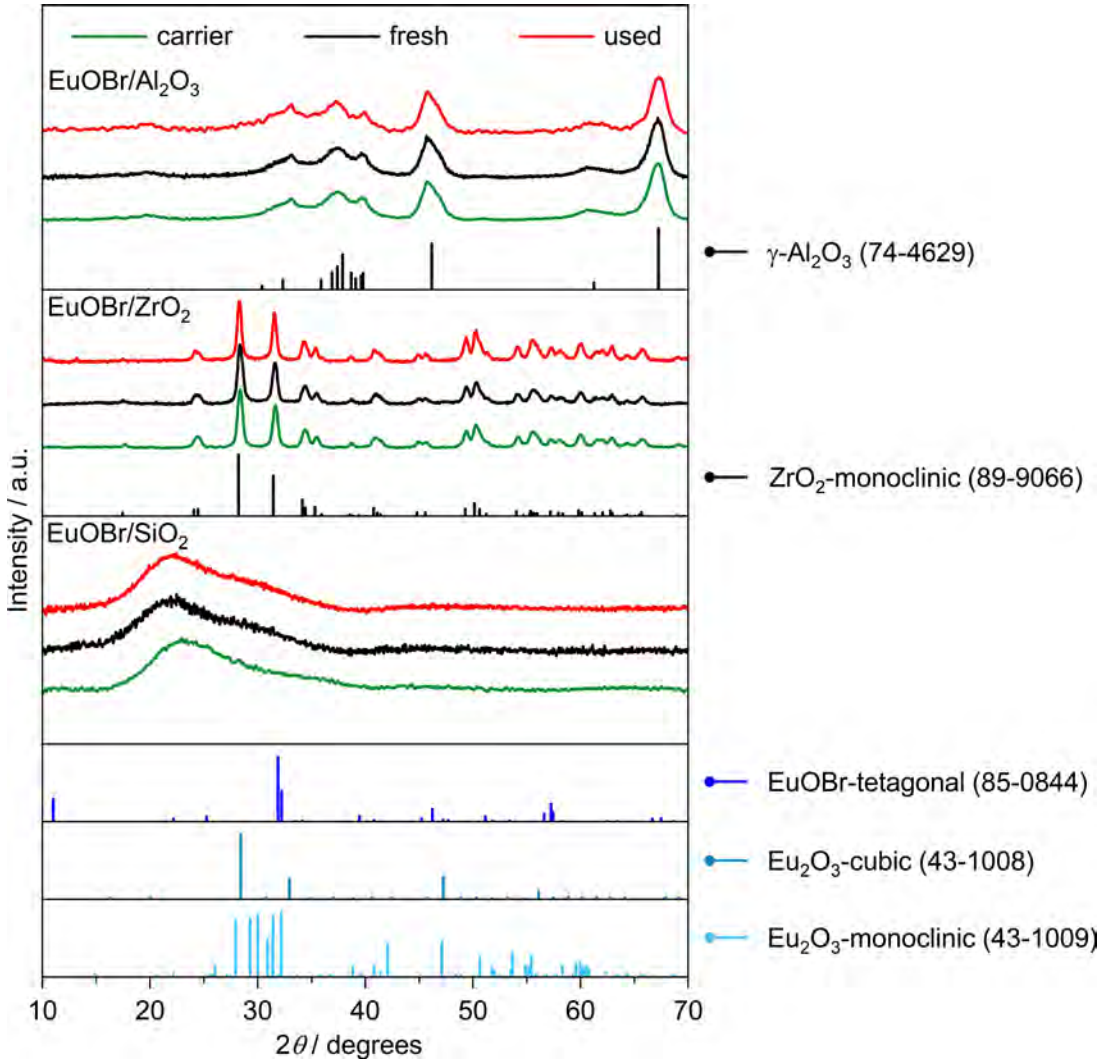

Figure S15. X-ray diffractograms of γ-Al_2O_3, ZrO_2, and SiO_2 carriers (green) and EuOBr/Al_2O_3, EuOBr/ZrO_2, and EuOBr/SiO_2 catalysts in fresh form (black) and after HBr oxidation (red) shown in **Figure 4a** of the main manuscript. Reference patterns shown as vertical lines below the measured diffractograms are identified on the right with their ICDD-PDF numbers. XRD patterns of fresh and used catalysts were identical to those of the bare carriers, with no observable contributions from Eu_2O_3 and EuOBr, indicating a high dispersion of the active phase.

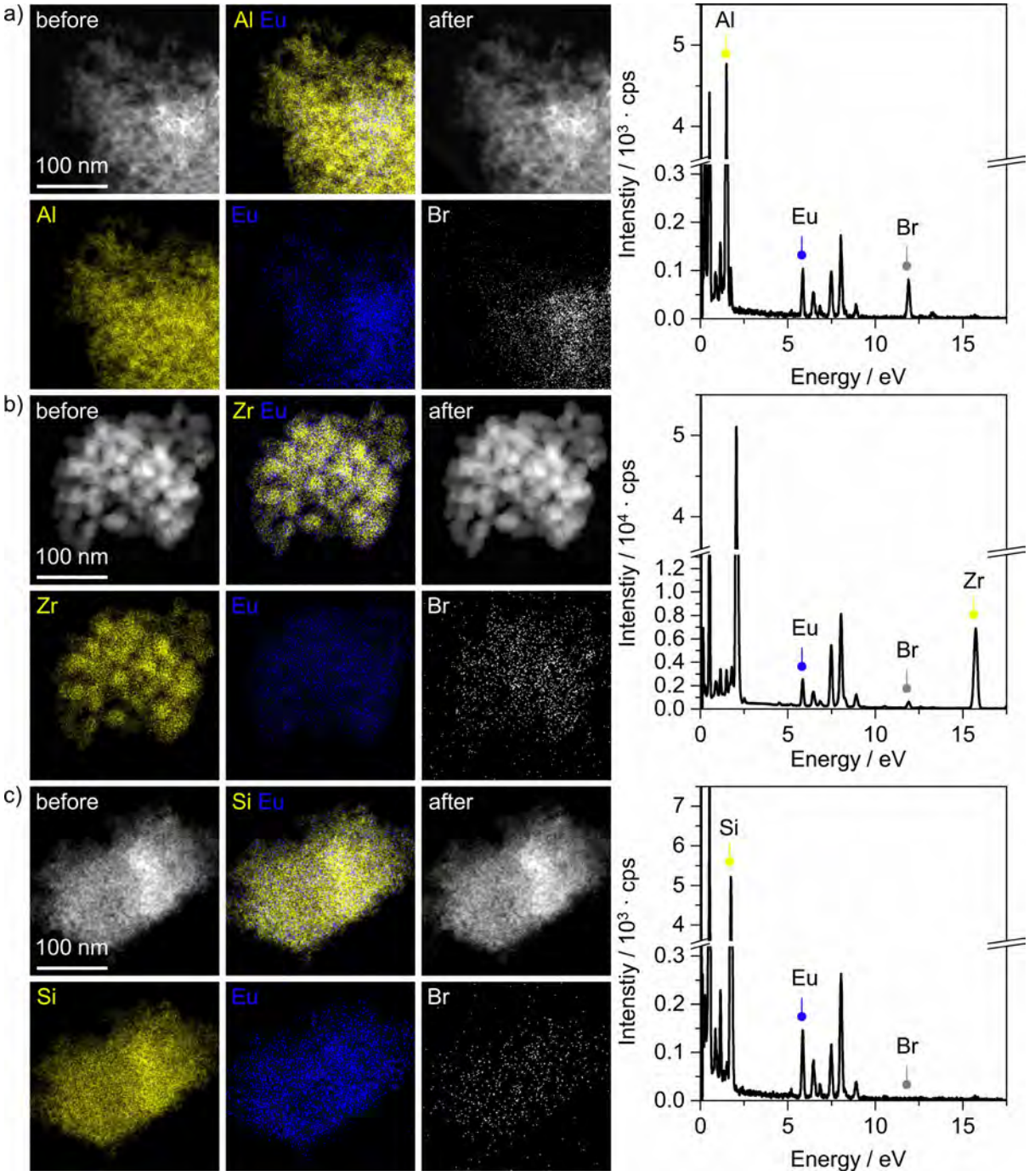

Figure S16. Elemental maps of the a) EuOBr/Al_2O_3, b) EuOBr/ZrO_2, and c) EuOBr/SiO_2 catalysts used in the HBr oxidation tests shown in **Figure 4a** of the main manuscript. The signals used for detecting the elements are indicated in the representative X-ray spectra on the right. The similar morphology observed in the HAADF-STEM micrographs before and after elemental mapping confirms the stability of the samples under the electron beam. The active phase is observed to be finely dispersed on the carrier, in line with the XRD data presented in **Figure S15**. Comparison of the relative intensity of Br and Eu signals indicates a decrease in Br:Eu ratio in the order: EuOBr/Al_2O_3 > EuOBr/ZrO_2 >> EuOBr/SiO_2, which coincides with the activity trend observed in HBr oxidation.

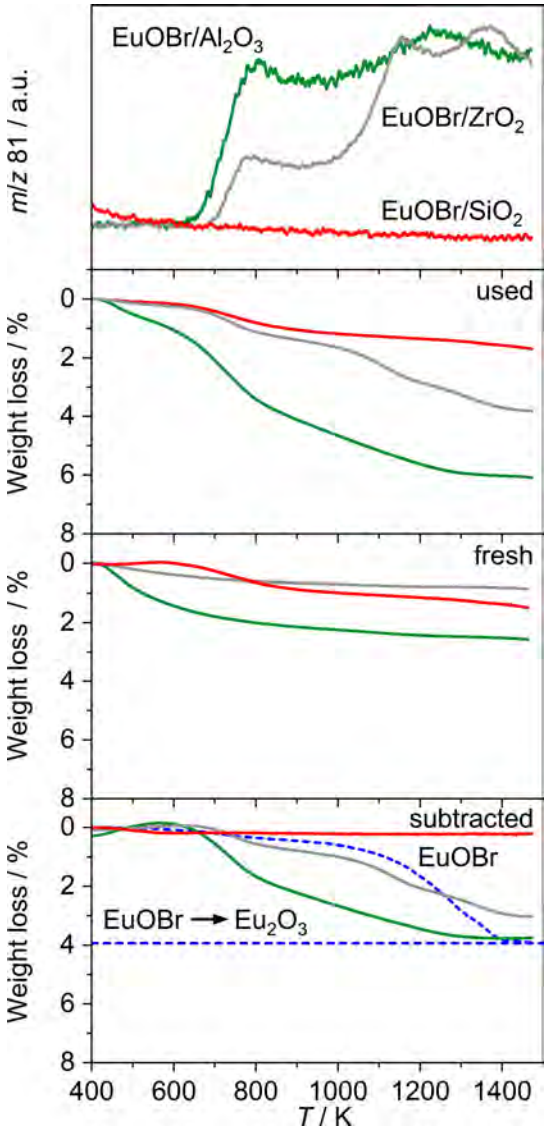

Figure S17. Thermogravimetric analysis of EuOBr/Al_2O_3, EuOBr/ZrO_2, and EuOBr/SiO_2 catalysts in fresh form and after the HBr oxidation tests presented in **Figure 4a** of the main manuscript and Br_2 evolution signals evidenced for the used samples. The bottom plot was obtained by subtracting the weight loss profile of the precursor from that of the used catalyst to isolate the weight loss associated with the supported phase, assuming that the carrier is not affected by the reaction. The horizontal dashed line indicates the predicted weight loss upon complete transformation of the active phase to EuOBr. Only the EuOBr/Al_2O_3 displays a weight loss of similar magnitude, while the EuOBr/ZrO_2 catalyst shows a slightly lower weight loss. In contrast, the minimal weight loss observed in the case of EuOBr/SiO_2 suggests almost no bromination, which is in line with the EDXS mapping shown in **Figure S16**. The type of carrier is also seen to impact the temperature of re-oxidation, with EuOBr/Al_2O_3 displaying a significant reduction compared to that predicted for the bulk EuOBr if no support effect was present (blue dashed line). This result indicates an enhancement of the bromine evolution in the presence of Al_2O_3 and is in good agreement with the high activity of EuOBr/Al_2O_3 in HBr oxidation (**Figure 4a** of the main manuscript).

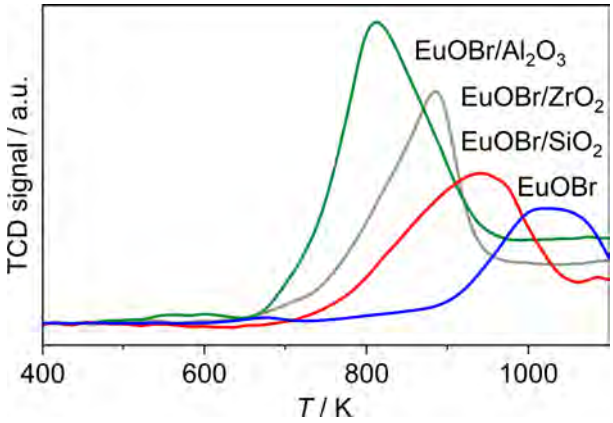

Figure S18. Temperature-programmed reduction with hydrogen (H_2-TPR) profiles of $EuOBr/Al_2O_3$, $EuOBr/ZrO_2$, and $EuOBr/SiO_2$ catalysts after the HBr oxidation tests presented in **Figure 4a** of the main manuscript. The H_2-TPR profile of bulk EuOBr is shown for comparison. TCD signals are normalized with respect to the Eu content in the sample. The position of the low-temperature reduction peak (520-700 K) indicates that the oxidizing potential of the catalysts decreases in the order $EuOBr/Al_2O_3$ > $EuOBr/ZrO_2$ ≈ EuOBr > $EuOBr/SiO_2$, which is in very good agreement with the order of activity in HBr oxidation.

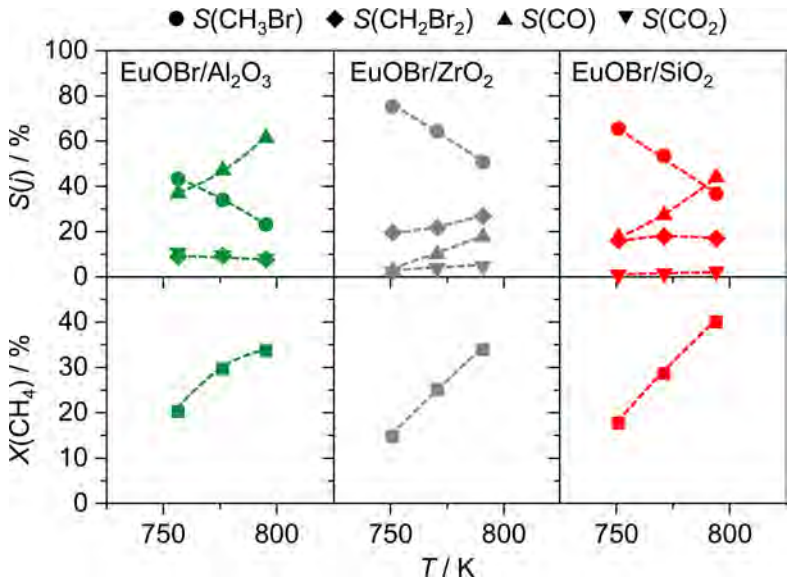

Figure S19. Conversion of methane and product selectivity *versus* temperature in MOB over $EuOBr/Al_2O_3$, $EuOBr/ZrO_2$, and $EuOBr/SiO_2$ catalysts. Conditions: CH_4:HBr:O_2:Ar:He = 6:6:3:4.5:80.5, F_T/W_{cat} = 100 $cm^3\ min^{-1}\ g_{cat}^{-1}$, P = 1 bar.

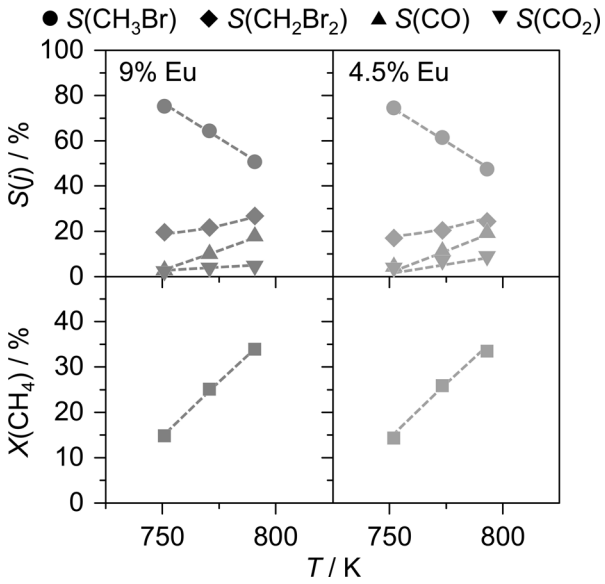

Figure S20. Conversion of methane and product selectivity *versus* temperature in MOB over $EuOBr/ZrO_2$ catalyst for two Eu loadings of 9 wt.% and 4.5 wt.%. Conditions: CH_4:HBr:O_2:Ar:He = 6:6:3:4.5:80.5, F_T/W_{cat} = 100 $cm^3\ min^{-1}\ g_{cat}^{-1}$, P = 1 bar. Decreasing the Eu content from 9 wt.% to 4.5 wt.% led to a very similar conversion of methane and selectivity to CH_3Br.